Nanoscale Advances

ROYAL SOCIETY OF CHEMISTRY

PAPER

View Article Online
View Journal | View Issue

Cite this: *Nanoscale Adv.*, 2025, **7**, 8058

Hemoglobin-loaded ZIF-8 nanoparticles functionalized with human serum albumin as stealth, stable, and biocompatible oxygen carriers

Despoina Douka, † Arnau Dieste-Izquierdo, † Clara Coll-Satue, Eva Jakljevič, Fernando Enrique Farfán-Esponda, Ana María Pablo Sainz-Ezquerra and Leticia Hosta-Rigau *

Hemoglobin-based oxygen carriers (HBOCs) offer a promising alternative to transfusions with donor red blood cells (RBCs), particularly in emergency and battlefield settings where blood availability and storage pose significant challenges. However, the clinical translation of HBOCs has been hindered by issues related to structural instability, immune clearance, and impaired hemoglobin (Hb) functionality. To address these limitations, we developed a next-generation HBOC by encapsulating Hb within zeolitic imidazolate framework-8 (ZIF-8) nanoparticles (NPs) (Hb@ZIF-8 NPs) and functionalizing the surface with a covalently bound layer of human serum albumin (HSA)—the most prevalent protein in human plasma. This strategy—employing a poly-L-lysine bridging step and glutaraldehyde crosslinking—resulted in HSA-coated Hb@ZIF-8 NPs with high Hb loading, enhanced colloidal stability in physiologically relevant media, and reduced opsonin adsorption. Compared to PEGylated controls, HSA-coated Hb@ZIF-8 NPs demonstrated superior stealth properties, including minimal IgG binding and preserved dysopsonin (*i.e.*, bovine serum albumin) association. Spectroscopic analyses and oxygen dissociation measurements confirmed that encapsulated Hb retained oxygen-binding and -release capabilities with cooperative behavior. Furthermore, cytotoxicity assays in macrophage cultures revealed improved biocompatibility relative to previously reported ZIF-8-based HBOCs. These findings highlight the potential of HSA-functionalized Hb@ZIF-8 NPs as a safe and effective platform for oxygen delivery, supporting their further development for transfusion medicine and acute care applications.

Received 12th July 2025
Accepted 28th October 2025

DOI: 10.1039/d5na00677e

rsc.li/nanoscale-advances

1. Introduction

Blood transfusion therapy plays a vital role in saving millions of lives each year. However, the limited shelf life and stringent storage requirements of donor red blood cells (RBCs) present considerable challenges to maintaining a stable blood supply.[1] This issue is particularly critical in emergency and battlefield scenarios, where rapid and efficient medical intervention is essential.[2]

Hemoglobin-based oxygen carriers (HBOCs) have emerged as promising alternatives to donor RBCs, providing a rapid means of restoring oxygen delivery to vital organs. Unlike traditional blood transfusions, HBOCs offer several key advantages, including universal compatibility, sterility, prolonged storage stability, and ease of transport.[3,4] Despite these benefits, the clinical development of HBOCs has been hindered by the need to mitigate the harmful effects of free hemoglobin (Hb) in the bloodstream.[5] This challenge is typically addressed through chemical modifications or encapsulation techniques aimed at stabilizing Hb.[2,6,7] Key strategies for improving HBOC stability include polymerization,[8] conjugation with poly(ethylene glycol) (PEG) or oligosaccharides,[9] and encapsulation within liposomes.[10] Each of these strategies aims to stabilize Hb and increase its molecular size thereby preventing extravasation through blood vessel walls. However, chemical modifications such as polymerization and conjugation can compromise structural flexibility, potentially impairing its ability to bind and release oxygen efficiently.[11,12] While liposomal encapsulation has minimal impact on oxygen transport properties, a major drawback is the low encapsulation efficiency (EE) of Hb, which impedes scalability and commercial viability.[13] These constraints highlight the urgent need for next-generation Hb nanoparticles (NPs) with improved uniformity, higher Hb content, and enhanced EE while preserving optimal oxygen-binding and release characteristics.[14,15]

Recently, our team developed a straightforward, rapid and scalable method for synthesizing HBOCs with a high functional Hb content.[16] This approach employs zeolitic imidazolate framework-8 (ZIF-8), a well-known metal–organic framework (MOF), for Hb encapsulation.[17] ZIF-8 is particularly well-suited

Department of Health Technology, Technical University of Denmark, 2800 Kongens Lyngby, Denmark. E-mail: leri@dtu.dk

† These authors contributed equally.

for this application due to its high porosity, which facilitates oxygen transport, and its excellent biocompatibility.[16,18]

Given that native RBCs can survive in circulation for up to 120 days, achieving prolonged *in vivo* circulation time is a key goal for HBOC development.[19,20] Tissue-resident macrophages in organs such as the liver, spleen, lungs, and inflamed tissues play a central role in clearing foreign substances, including intravenously administered NPs like HBOCs.[21] Thus, previous generations of HBOCs have exhibited short circulation half-lives, limiting their practical application.[1,2] Such a clearance process is mediated by opsonins—serum proteins such as immunoglobulins, complement components, and coagulation proteins—that form a "biomolecular corona" around the NPs, marking them for macrophage recognition and removal.[22] PEG, an electrically neutral, hydrophilic, and highly biocompatible polymer, has been shown to reduce opsonin adsorption and it is widely regarded as the gold standard for extending the circulation time of nanoscale carriers.[21] However, PEG immunogenicity has become an increasingly recognized concern. Due to widespread exposure to PEG in food and personal care products, a significant portion of the population has developed anti-PEG antibodies.[23] These antibodies can trigger adverse effects such as accelerated blood clearance and hypersensitivity reactions upon exposure to PEGylated therapeutics, potentially compromising their efficacy and safety.[23] As a result, there is growing interest in alternative surface modification strategies.

Albumin, the most abundant serum protein, is an attractive alternative due to its inherent biological compatibility, high solubility, long circulatory half-life, and ability to act as a dysopsonin.[22] Dysopsonins binding prevents opsonin adsorption, thereby enhancing the stealth properties of NPs and decreasing their clearance by macrophages.[22] Several studies have demonstrated that an albumin corona around the NPs can effectively shield them from immune recognition, prolonging their circulation time.[22,24,25]

In this study, we present an improved version of our previously developed Hb-loaded ZIF-8 NPs (Hb@ZIF-8 NPs), featuring a covalently bound layer of human serum albumin (HSA) to enhance their stability, biocompatibility and circulation time. By anchoring HSA on the NPs surface, we aim to minimize opsonin adsorption and reduce macrophage-mediated clearance (Scheme 1). This innovative approach holds significant potential for overcoming the limitations of current HBOC formulations, paving the way for safer and more effective oxygen carriers.

2. Materials and methods

2.1. Materials

Zinc nitrate hexahydrate ($Zn(NO_3)_2 \cdot 6H_2O$), iron(III) chloride hexahydrate ($FeCl_3 \cdot 6H_2O$), 2-methylimidazole (HmIm), tannic acid (TA), ethylenediaminetetraacetic acid (EDTA) solution (0.5 M), sodium lauryl sulfate (SLS), PEG (–OH terminated, M_W 6000 Da), glutaraldehyde (GA) solution (25% in water), poly-L-lysine hydrobromide (PLL, M_W 30–70 kDa), HSA in lyophilized powder, bovine serum albumin (BSA) in lyophilized powder, fluorescein 5(6) – isothiocyanate (FITC), FITC labelled immunoglobulin G (IgG-FITC) from human serum, potassium hexacyanoferrate(III) ($K_3[Fe(CN)_6]$), sodium chloride (NaCl), sodium dithionite (SDT), sodium bicarbonate ($NaHCO_3$), 4-(2-hydroxyethyl)piperazine-1-ethane-sulfonic acid (HEPES), tris(hydroxymethyl)aminomethane (TRIS), phosphate buffered saline (PBS), Dulbecco's phosphate buffered saline (DPBS), penicillin/streptomycin, fetal bovine serum (FBS) and Hb from bovine blood in lyophilized powder form were purchased from Merck Life Sciences A/S (Søborg, DK). Dimethylsulfoxide (DMSO) was purchased by VWR International A/S (Søborg, DK). Antifoaming agent was acquired from TCS Scientific Corp (PA, USA) and Dulbecco's Modified Eagle Medium (DMEM) was purchased from ThermoFisher Scientific (Waltham, USA). CellTiter-Glo® luminescent cell viability (CV) assay was obtained from Promega Corporation (Madison, USA) and bovine blood with citrate was obtained from SSI Diagnostica A/S (Hillerød, DK). The RAW 264.7 murine macrophage cell line was purchased from European Collection of Authenticated Culture Collections (ECACC, Wiltshire, UK).

Dialysis was performed using high-retention seamless cellulose dialysis tubing (32 mm width, 12.4 kDa MWCO) purchased from Merck Life Sciences A/S (Søborg, DK). A saline solution (0.9% NaCl) was prepared using ultrapure water (Mili-Q (MQ), gradient A 10 system, TOC < 4 ppb, resistance 18 MV cm, EMD Millipore).

2.2. Hb extraction from bovine blood

Hb was extracted following a previous report.[26] In brief, bovine blood was washed (3×, 2000*g*, 20 min, 4 °C) with a saline solution (0.9% NaCl, 1 : 1 v/v ratio) in an ice bath using a high-speed centrifuge (SL16R centrifuge, ThermoScientific, Hvidovre, DK). After centrifugation, the supernatant containing the plasma was discarded, and the resulting pellet of RBCs was collected and washed in PBS (3×, 10 956*g*, 5 min, 4 °C) to remove remaining plasma components. After the last centrifugation step, the RBCs were resuspended in 15 mL of MQ and left overnight at 4 °C to induce release of Hb due to osmotic cell lysis. The lysate was centrifuged (10 000*g*, 20 min, 4 °C) to remove residual cell debris and the supernatant containing stroma-free Hb was collected, filtered using a disposable filter funnel, aliquoted and stored at −80 °C. The Hb concentration was determined using our previously reported SLS-based method.[27]

2.3. Fabrication and characterization of PLL- and HSA-coated Hb@ZIF-8 NPs (Hb@ZIF-8/PLL/HSA NPs)

2.3.1. Fabrication of Hb@ZIF-8 NPs. Hb@ZIF-8 NPs were synthesized following a previously reported protocol from our group.[16] Briefly, HmIm (40 μL, 2 M in MQ), Hb (568 μL, 140.8 mg mL^{-1} in MQ), and PEG (333 μL, 1200 mg mL^{-1} in MQ) were mixed in an 8 mL glass vial under continuous stirring (800 rpm). MQ was then added to a final volume of 1.8 mL. Subsequently, $Zn(NO_3)_2 \cdot 6H_2O$ (200 μL, 0.1 M in MQ) was introduced into the mixture, which was further stirred at 800 rpm for 10 min. The resulting suspension was transferred to 2 mL Eppendorf tubes,

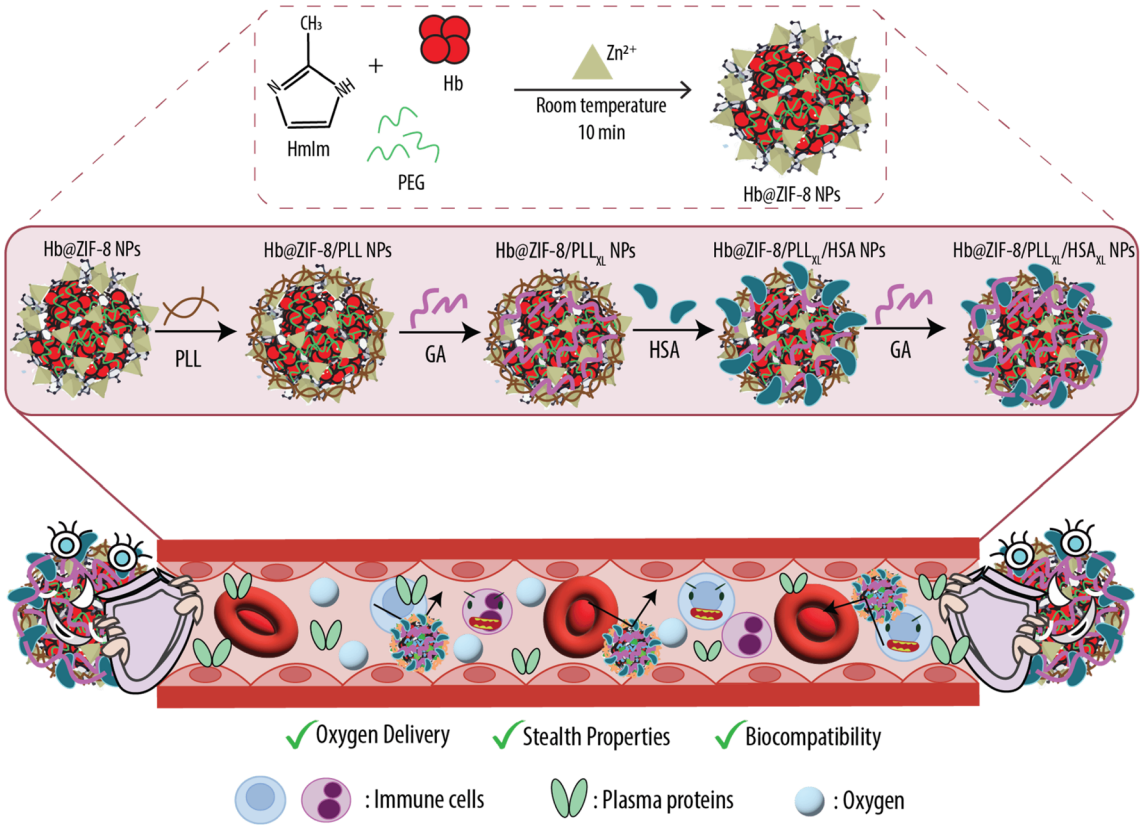

Scheme 1 Schematic illustration of Hb-loaded ZIF-8 NPs (Hb@ZIF-8 NPs) synthesized from zinc ions (Zn^{2+}), 2-methylimidazole (HmIm), Hb, and poly(ethylene glycol) (PEG), followed by coating with poly-L-lysine (PLL) and human serum albumin (HSA). Coating of Hb@ZIF-8 NPs with HSA protects against nonspecific protein adsorption and recognition by the immune system, while preserving the oxygen delivery function of Hb. The NPs are referred to as Hb@ZIF-8/PLL/HSA$_{XL}$ and Hb@ZIF-8/PLL$_{XL}$/HSA$_{XL}$ NPs, where the subscript 'XL' denotes crosslinking with glutaraldehyde (GA) following PLL or HSA deposition.

washed with MQ (3× 10 956*g*, 5 min, 4 °C) and resuspended in 2 mL. The Hb@ZIF-8 NPs were stored at 4 °C until further use.

2.3.2. Fabrication of Hb@ZIF-8/PLL/HSA NPs. For the synthesis of Hb@ZIF-8/PLL/HSA NPs, various solvents were evaluated first (*i.e.*, MQ, 10 mM HEPES pH 7.4, 10 mM HEPES pH 8.5, 25 mM HEPES pH 7.4, 25 mM HEPES pH 8.5, 25 mM HEPES pH 7.4 with 150 mM NaCl, and 25 mM HEPES pH 8.5 with 150 mM NaCl). For that, Hb@ZIF-8 NPs (containing 10 mg Hb) were dispersed in a 4 mL glass vial, followed by the addition of PLL (600 μL, 10 mg mL^{-1}) and additional solvent to reach a final volume of 3 mL. The mixture was incubated in a rotor (40 rpm, 10 min), transferred into two 1.5 mL Eppendorf tubes and washed with the corresponding solvent (2× 10 956*g*, 5 min). After centrifugation, the suspension was transferred to a 4 mL glass vial, mixed with HSA (600 μL, 10 mg mL^{-1}), and adjusted to a final volume of 3 mL with additional solvent. The suspension was incubated again under rotation (40 rpm, 10 min), transferred into two 1.5 mL Eppendorf tubes and washed (2× 10 956*g*, 5 min). For crosslinking, the suspension was adjusted to a final volume of 1.5 mL, transferred to a 4 mL glass vial, and incubated with GA (20 μL 0.8% in MQ) at 500 rpm using a magnetic stirrer and room temperature (RT) for up to 24 h. The final product was transferred to a 2 mL Eppendorf tube, washed (3×, 10 956*g*, 5 min), resuspended in 1.5 mL and stored at 4 °C.

To determine the optimal PLL and HSA concentrations for Hb@ZIF-8/PLL/HSA NPs preparation, the protocol described above was repeated using varying concentrations of PLL (300, 600, 1200, or 2400 μL, 10 mg mL^{-1}) and HSA (300, 600, 900, 1200 or 1500 μL, 10 mg mL^{-1}), with 10 mM HEPES pH 8.5 used as the solvent, while crosslinking was not required. For crosslinking time optimization, the washed suspension after HSA addition was incubated with GA (20 μL of 0.8% in MQ) while stirring at 500 rpm for up to 24 h at RT. For optimization of the Hb : GA molar ratio, the washed suspension after PLL addition was incubated with GA (1, 2, 10, or 20 μL of 0.8% in MQ, corresponding to 1 : 0.5, 1 : 1, 1 : 5, and 1 : 10 Hb : GA molar ratios) while stirring for 15 min at RT. Following crosslinking and washing, HSA was added as described, and a second crosslinking step using GA at the same concentrations was performed under identical conditions. The final product was washed (3×, 10 956*g*, 5 min), resuspended in 1.5 mL, and stored at 4 °C. Hb@ZIF-8/PLL/HSA NPs crosslinked with GA only after HSA deposition are referred to as Hb@ZIF-8/PLL/HSA$_{XL}$ NPs, while those undergoing two crosslinking steps are denoted as Hb@ZIF-8/PLL$_{XL}$/HSA$_{XL}$ NPs.

2.3.3. Zeta (ζ)-potential. The ζ-potential of the NPs was measured using a Zetasizer nanoseries nano-ZS (Malvern Panalytical Ltd, Malvern, UK) following an 80× dilution in MQ.

2.3.4. Cryo-scanning electron microscopy (Cryo-SEM). To assess the size and morphology of Hb@ZIF-8 and Hb@ZIF-8/PLL_{XL}/HSA_{XL} NPs while preserving the integrity of the protein coating, Cryo-SEM was performed using a Quanta FEG 200 Cryo-Environmental Scanning Electron Microscope (FEI Company, Hillsboro, US) equipped with a Cryo-preparation chamber and a Cryo-stage. A 5 μL aliquot of the NP suspension (100× diluted in MQ) was applied onto a brass Cryo-stub connected to a transfer rod. The sample was plunge-frozen in slush nitrogen and immediately transferred under a high vacuum to the Cryo-preparation chamber maintained at −180 °C.

To remove residual surface ice acquired during transfer, the sample was sublimated at −100 °C for 10 min in the SEM chamber maintained at −160 °C. Following sublimation, a thin platinum layer was sputter-coated onto the sample under an argon atmosphere for 30 s. Imaging was subsequently conducted in high vacuum mode using an accelerating voltage of 20.0 kV and particle size distribution was analyzed in ImageJ software by measuring approximately 150 and 530 NPs, for Hb@ZIF-8 and Hb@ZIF-8/PLL_{XL}/HSA_{XL} NPs, respectively.

2.3.5. Hb quantification, EE and loading content (LC). The concentration of encapsulated Hb within the different NPs was quantified using the SLS-Hb method.[27] Briefly, EDTA (60 μL, 50 mM in MQ) was added to a NP suspension (60 μL) followed by serial dilutions in MQ. A standard curve was prepared by diluting bovine Hb stock in MQ. Next, SLS (200 μL, 0.6 mg mL^{-1} in MQ) was dispensed in triplicate into a 96-well plate (Nunclon™ Delta Surface), followed by the addition of 10 μL of either the Hb standard or the NPs suspension. The plate was covered with aluminum foil and incubated on a plate shaker for 5 min at RT before measuring the absorbance (Abs) at 539 nm using a plate reader (Tecan Spark, Tecan Group Ltd, Männedorf, CH).

The EE and LC were calculated using the following equations:

$$\text{EE (\%)} = (\text{Hb concentration in Hb@ZIF-8 NPs})/(\text{Hb concentration initially added}) \times 100$$

The Hb concentration in the Hb@ZIF-8 NPs was determined using the SLS-Hb method, while the initial Hb concentration was 40 mg mL^{-1}.

$$\text{LC (\%)} = (\text{weight of Hb in Hb@ZIF-8 NPs})/(\text{weight of Hb@ZIF-8 NPs}) \times 100$$

2.3.6. Fourier-transform infrared (FTIR) spectroscopy. Attenuated total reflectance-FTIR spectra were acquired using a Bruker Alpha-P spectrometer (Bruker Corp., Massachusetts, USA). Free Hb, PLL, HSA and the synthetized NPs (*i.e.*, Hb@ZIF-8, Hb@ZIF-8/PLL/HSA_{XL} and Hb@ZIF-8/PLL_{XL}/HSA_{XL} NPs) were analyzed in powder form under ambient conditions across a spectral range of 398–3998 cm^{-1}. Each sample was measured with 32 scans to ensure data reproducibility and spectral quality. To minimize interference, background spectra were recorded in air before sample measurements.

2.4. Oxygen transporting properties

2.4.1. Quantification of released oxygen. The oxygen release capacity of free Hb, Hb@ZIF-8/PLL/HSA_{XL} and Hb@ZIF-8/PLL_{XL}/HSA_{XL} NPs was evaluated using a needle-type oxygen microsensor (PreSens, Regensburg, DK) as previously reported by our group.[28] Briefly, free Hb (600 μL, 1 or 4 mg mL^{-1}), Hb@ZIF-8/PLL/HSA_{XL} NPs (600 μL, 1 mg per mL Hb) or Hb@ZIF-8/PLL_{XL}/HSA_{XL} NPs (600 μL, 4 mg per mL Hb) were diluted in 10 mM HEPES buffer pH 8.5 and transferred to a 2 mL glass vial which was tightly closed with a rubber cap. The oxygen microsensor was inserted into the suspensions, and oxygen release was triggered by adding 50 μL of an aqueous 100 mg per mL $K_3[Fe(CN)_6]$ solution. This induced the oxidation of the ferrous ion (Fe^{2+}) in oxygenated Hb (oxyHb) to the ferric state (Fe^{3+}), converting oxyHb into metHb and thereby releasing oxygen, which was recorded by the sensor. The released oxygen concentration (μM) was calculated by subtracting the maximum value recorded after $K_3[Fe(CN)_6]$ addition from the baseline value measured just before incubation. For better comparison across samples, the resulting values were normalized to the amount of Hb (in mg) encapsulated in each NP formulation.

2.4.2. Reversible oxygen binding and release assessment. The ability of free Hb, Hb@ZIF-8/PLL/HSA_{XL} and Hb@ZIF-8/PLL_{XL}/HSA_{XL} NPs to reversibly bind and release oxygen was analyzed by UV-Vis spectrophotometry (UV-2600, Shimadzu Corporation, JP). The NPs were diluted in 10 mM HEPES buffer pH 8.5 to a final Hb concentration of 1 mg in 2.6 mL and transferred into a plastic cuvette. The cuvette was sealed with a lid, and the UV-Vis spectrum was recorded in the range of 350–650 nm.

To induce oxygen release, a pinch (∼2 mg) of SDT was added to the cuvette, and the lid was immediately closed before acquiring the next spectrum. Following spectrum recording, the cuvette was exposed to a direct flow of compressed air for 10 min, after which a new spectrum was recorded. A second pinch of SDT was then added to the solution, and another spectrum was obtained, completing two full oxygen binding and release cycles.

2.4.3. Oxygen dissociation curve (ODC). The ODCs from free Hb, Hb@ZIF-8/PLL/HSA_{XL} and Hb@ZIF-8/PLL_{XL}/HSA_{XL} NPs were acquired using a HEMOX Analyzer (TCS Scientific Corp., New Hope, PA, USA). The different suspensions were diluted in 10 mM HEPES pH 7.4 to a final Hb concentration of 3 mg per mL Hb and a total volume of 3 mL, and 6 μL of anti-foaming agent was added to each sample. Measurements were performed at 37 °C while purging the suspensions with compressed air and nitrogen gas to obtain oxyHb and deoxygenated Hb (deoxyHb), respectively. The partial oxygen pressure (pO_2) at which Hb is 50% saturated ($p50$) and the Hill coefficient (n_H) were obtained using the pre-installed software (TCS HEMOX DAQ System).

2.5. Stability assessment in different solvents

To assess the stability of uncoated Hb@ZIF-8, Hb@ZIF-8/PLL/HSA_{XL} and Hb@ZIF-8/PLL_{XL}/HSA_{XL} NPs in different solvents, including physiologically relevant media, 1 mg of NPs was

incubated in 500 μL of various media (*i.e.*, MQ, 0.9% NaCl, 25 mM HEPES pH 7.4, 10 mM HEPES pH 8.5, 10 mM HEPES pH 7.4 with 150 mM NaCl, 10 mM TRIS pH 7.4 with 150 mM NaCl, PBS and DMEM). The suspensions were stored at 4 °C for 1 h, 4 h, 1 day and 7 days, except those in DMEM, which were incubated at 37 °C. At each time point, the NPs were centrifuged, and a photographic image of the pellet was taken. Next, 10 μL of the supernatant was analyzed for potential Hb measuring UV-Vis spectra in the range of 190–840 nm using a NanoDrop 2000c (ThermoFisher Scientific, Walthman, USA). For this, a 3 μL aliquot was placed on the NanoDrop pedestal and the spectrum was obtained. Afterward, the pellet was resuspended in the corresponding supernatants and stored until the next time point. Hb loss at each time point was quantified using a standard curve generated from a bovine blood-derived Hb stock solution measured at 413 nm using the NanoDrop (Fig. S1, SI). The percentage of Hb released was calculated using the following formula:

$$\text{Hb released (\%)} = (\text{Hb loss at each time point/initial Hb content in the NPs}) \times 100$$

The initial Hb content within the Hb@ZIF-8/PLL/HSA_{XL} and Hb@ZIF-8/PLL_{XL}/HSA_{XL} NPs was determined using the SLS-Hb method by subtracting the amount of Hb released after GA crosslinking from the amount measured following fabrication but prior to crosslinking. For Hb@ZIF-8 NPs, the initial Hb content was determined directly after fabrication using the SLS-Hb method.

2.6. Stealth properties evaluation

2.6.1. Synthesis of PEG-coated Hb@ZIF-8 NPs (Hb@ZIF-8/PEG NPs). The fabrication of Hb@ZIF-8/PEG NPs was conducted following a previously established protocol.[17] Briefly, Hb@ZIF-8 NPs (1 mg, MQ pH 8.5) were rapidly mixed with TA (20 μL, 40 mg mL^{-1} in MQ) and vortexed for 5 s. Next, $FeCl_3$ (1.2 μL, 12.5 mg mL^{-1} in MQ) was added, and the suspension was vortexed for another 5 s. MQ at pH 8.5 was added to reach a final volume of 1 mL. The resulting TA-coated Hb@ZIF-8 NPs were washed with MQ at pH 8.5 (3×, 10 956*g*, 5 min, 4 °C) using a high-speed centrifuge. Next, the NPs (1 mg in PBS) were incubated with PLL (60 μL, 10 mg mL^{-1} in PBS) and PBS, which was added to a final volume of 300 μL for 15 min at RT while rotating at 40 rpm. The NPs were washed with PBS (2×, 10 956*g*, 5 min, 4 °C) and subsequently incubated with PEG (60 μL, 10 mg mL^{-1} in PBS) and PBS, which was added to a final volume of 300 μL also for 15 min at RT while rotating at 40 rpm. The final Hb@ZIF-8/PEG NPs were washed with PBS (3×, 10 656*g*, 5 min, 4 °C) and stored at 4 °C for further studies.

2.6.2. Synthesis of FITC-labelled BSA (BSA-FITC). The synthesis of BSA-FITC was conducted following a previously reported protocol.[29] Briefly, FITC (1 mL, 10 mg mL^{-1} in DMSO) was added dropwise to a BSA solution (20 mL, 5 mg mL^{-1} in 50 mM $NaHCO_3$, pH 10) and incubated overnight in the dark, covered with aluminum foil, at 40 rpm using a rotor. Unbound FITC was removed by dialysis (12.4 kDa MWCO) against MQ for 3 days, and the purified BSA-FITC was lyophilized and stored at −20 °C.

2.6.3. Assessment of IgG-FITC and BSA-FITC adsorption. Suspensions of the different NPs (*i.e.*, Hb@ZIF-8/PLL/HSA_{XL}, Hb@ZIF-8/PLL_{XL}/HSA_{XL} and Hb@ZIF-8/PEG NPs) (300 μL, 0.5, 1 or 2 mg mL^{-1} in 10 mM HEPES pH 7.4 with 150 mM NaCl) were incubated with IgG-FITC (7.5 μL, 20 mg mL^{-1} in 0.01 M PBS pH 7.4, containing 15 mM sodium azide) and BSA-FITC (15 μL, 10 mg mL^{-1} in 10 mM HEPES pH 7.4 150 mM NaCl) for 4 h at 37 °C in a thermoshaker (PHMT Thermoshaker, Grant-bio, SP). Following incubation, the NPs were washed with 10 mM HEPES pH 7.4 with 150 mM NaCl (2×, 12 000*g*, 5 min, RT) to remove any unbound protein. The supernatants were collected in Eppendorf tubes for further analysis. The fluorescence intensity of the supernatants due to unbound proteins was analyzed with a plate reader (Tecan Spark, Tecan Group Ltd, Männedorf, CH) at excitation and emission wavelengths of 493 and 516 nm, respectively.

2.7. Biocompatibility assessment

The biocompatibility of Hb@ZIF-8/PLL_{XL}/HSA_{XL} NPs was evaluated using a luminescent-based CV assay. RAW 264.7 macrophage cells were cultured in DMEM with 10% FBS and penicillin/streptomycin (1% v/v, 10 000 U mL^{-1} and 10 μg mL^{-1}, respectively) and maintained in a humidified incubator at 37 °C with 5% CO_2. Once the cells reached 70–80% confluency, they were sub-cultured by washing with DPBS and detaching using a cell scraper.

To assess the CV, 3×10^5 RAW 264.7 cells per well were seeded into a transparent 96-well plate and incubated at 37 °C with 5% CO_2 for 24 h. The following day, the cells were exposed to increasing concentrations of Hb@ZIF-8/PLL_{XL}/HSA_{XL} NPs (100 μL, 0–5 mg mL^{-1}) for an additional 24 h. After incubation, the cells were washed with DPBS (2×, 100 μL) and treated with 100 μL CellTiter-Glo® solution, prepared by dissolving lyophilized CellTiter-Glo® Substrate in 10 mL of CellTiter-Glo® Buffer. The plates were shaken for 2 min and incubated at RT for an additional 10 min. Subsequently, the contents of each well were transferred to a white 96-well plate. CellTiter-Glo® solution alone (without cells) was used as a negative control, while untreated cells served as a positive control. Luminescence was measured using the plate reader at an integration time of 1 s. All experimental conditions were evaluated in technical triplicates over three independent experiments, and the normalized CV (nCV) was calculated using the following equation:

$$\text{nCV (\%)} = (\text{experimental value} - \text{negative control value})/(\text{positive control value} - \text{negative control value}) \times 100\%$$

2.8. Statistical analysis

For comparisons with respect to a control, a one-way ANOVA followed by Dunnett's test was applied. Comparisons between two independent groups were assessed using the Mann–Whitney test. In all cases, statistical significance was set at $\alpha = 0.05$.

Analyses were performed using GraphPad Prism (version 10.6.0 (890)).

3. Results and discussion

3.1. Fabrication and characterization of Hb@ZIF-8/HSA NPs

Our group has pioneered a simple and efficient one-pot method for encapsulating Hb within ZIF-8 NPs.[16,17] As previously reported, the resulting Hb@ZIF-8 NPs exhibit an exceptionally high functional Hb concentration of 36 mg mL^{-1}, evidenced by their ability to reversibly bind and release oxygen. As shown in Fig. 1a, these NPs possess a slightly negative charge of -6.6 ± 0.7 mV and a remarkable EE and LC of 89 and 98.8%, respectively.[17] Morphological analysis *via* Cryo-SEM reveals homogeneous, rounded, and well-defined NPs with an average size of 127 ± 26 nm.

RBCs have an average lifespan of approximately 120 days in circulation.[1] However, achieving a comparable circulation time for HBOCs remains challenging due to the systemic clearance of NPs, which are prone to opsonin binding and subsequent removal by the mononuclear phagocyte system (MPS).[25] A common strategy to mitigate MPS clearance involves coating NPs with a hydrophilic layer that reduces protein adsorption.[25] Thus, to enhance circulation time and minimize immunogenicity, we previously modified Hb@ZIF-8 NPs with a PEG coating—a widely used synthetic polymer that prevents opsonization and MPS-mediated clearance.[17,25] Our findings demonstrated that Hb@ZIF-8/PEG NPs effectively reduced IgG adsorption while enhancing BSA deposition, a key dysopsonin.[17] Moreover, Hb@ZIF-8/PEG NPs exhibited favorable biocompatibility in hemolysis and CV assays. *In vivo* studies in mice further confirmed an enhanced circulation time, with Hb@ZIF-8/PEG NPs displaying a half-life of 14.8 h, compared to only 7.65 h for free Hb.[18]

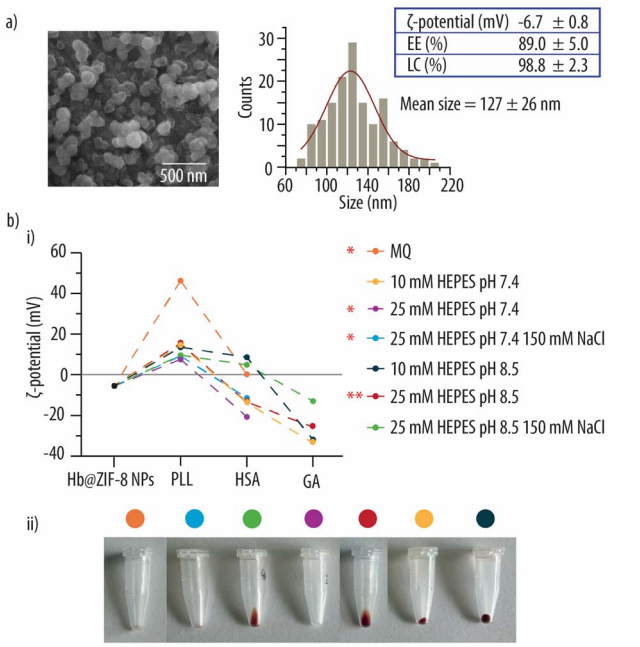

Fig. 1 (a) Cryo-SEM micrograph and corresponding size histogram of Hb-loaded ZIF-8 NPs (Hb@ZIF-8 NPs). Zeta (ζ)-potential, encapsulation efficiency (EE) and loading content (LC) are also reported. (b) (i) ζ-potential measurements of Hb@ZIF-8 NPs after sequential deposition of poly-L-lysine (PLL), human serum albumin (HSA) and crosslinking with glutaraldehyde (GA) in MQ and HEPES buffer at varying concentrations, pH conditions, and with or without NaCl. Buffers marked with a red asterisk indicate disassembly of the NPs, while double red asterisks denote NP agglomeration. (ii) Photographic images of Hb@ZIF-8 NPs coated with PLL, HSA and crosslinked with GA after two washes in: MQ (orange), 25 mM HEPES pH 7.4 with NaCl (blue), 25 mM HEPES pH 8.5 with NaCl (green), 25 mM HEPES pH 7.4 (purple), 25 mM HEPES pH 8.5 (red), 10 mM HEPES pH 7.4 (yellow) and 10 mM HEPES pH 8.5 (dark blue). PLL and HSA were used at concentrations of 2 mg mL^{-1}, and GA was applied at a 1 : 10 molar ratio relative to Hb. All NPs were incubated with GA for 4 h.

Although PEG coatings remain widely used to prevent NP aggregation, opsonization, and phagocytosis—thereby extending systemic circulation—the increasing prevalence of anti-PEG antibodies in the population has raised concerns about PEG-related immunogenicity.[23] In this context, HSA has emerged as a promising surface-modifying alternative to PEG due to its ability to prevent opsonin adsorption. Albumin is the most abundant protein in human serum, playing a crucial role in the transport of nutrients and hydrophobic drugs in circulation.[25,30] More importantly, it functions as a dysopsonin for foreign NPs, reducing the binding of opsonins that promote MPS uptake and thereby prolonging NPs circulation time.[22,25,31] Thus, we explore the potential of HSA as a coating for our previously reported Hb@ZIF-8 NPs.[16–18]

Given that both Hb@ZIF-8 NPs and HSA are negatively charged at pH values close to physiological conditions (with HSA having an isoelectric point (pI) of 4.7), a positively charged PLL layer was introduced to achieve charge reversal. PLL, a cationic biopolymer composed of L-lysine—a naturally occurring amino acid—has a pI of ~10.5 and contains primary amine side chains that can capture protons, becoming positively charged at pH values below 10.5.[32,33] This high positive charge density makes PLL an ideal bridging agent between Hb@ZIF-8 NPs and HSA. Since HSA adsorption onto the NPs surface occurs through reversible interactions, a crosslinking step was introduced to prevent protein detachment. This stabilization was achieved using GA, which is commonly used in biological applications due to its ability to rapidly form covalent bonds under ambient conditions with primary amine groups in biomolecules through Schiff base formation. GA is a 5-carbon dialdehyde that reacts with primary amines, effectively crosslinking HSA and PLL to ensure a stable coating on Hb@ZIF-8 NPs. GA has been effectively utilized in previously reported HBOC formulations due to its high crosslinking efficiency, inducing stable crosslinking between Hb molecules and resulting in a robust formulation.[34,35] The successful deposition of both PLL and HSA was confirmed by monitoring ζ-potential changes. Various solvents (*i.e.*, both MQ and HEPES buffer at different concentrations, pH values, and with or without NaCl) were evaluated to identify the optimal solvent for maximum PLL and HSA deposition (Fig. 1b(i)). Following incubation with PLL (2 mg mL^{-1}), the ζ-potential increased across all tested buffers (from −6 mV for uncoated Hb@ZIF-8 NPs to +7–15 mV), with

the highest increase observed in MQ (+40 mV). This sharp rise in ζ-potential is likely due to the low pH of MQ (6.0–6.5), which further protonates PLL, enhancing its positive charge. These results indicate the successful incorporation of PLL in all tested conditions. Subsequent HSA (2 mg mL^{-1}) addition led to a decrease in ζ-potential across all conditions, though the extent varied. However, photographic images revealed that under certain conditions (*i.e.*, MQ, 25 mM HEPES pH 7.4, and 25 mM HEPES pH 7.4 with 150 mM NaCl), NPs disassembly occurred, likely due to HSA competing with the Zn^{2+} ions constituting the ZIF-8 core (Fig. 1b(ii)). Additionally, at 25 mM HEPES pH 8.5, the NPs formed aggregates that were difficult to resuspend. To further stabilize the coating, Hb@ZIF-8/PLL/HSA NPs were incubated in GA for crosslinking. As expected, this resulted in an additional decrease in ζ-potential, as GA reacts with free amino groups. Among the two buffer conditions that led to the most significant ζ-potential reduction, 10 mM HEPES pH 8.5 was selected for further optimization (from now on referred to as HEPES), given the reported GA higher crosslinking activity at pH values between 8 and 8.5.[36]

The optimal PLL and HSA concentrations were further determined using ζ-potential measurements (Fig. 2a). Incubation of Hb@ZIF-8 NPs with 1 mg per mL PLL resulted in a ~38 mV increase in ζ-potential, whereas doubling the PLL concentration to 2 mg per mL led to only a slight additional increase of 1.3 mV (Fig. 2a(i)). Further increasing the PLL concentration resulted in a decreased ζ-potential, indicating that the Hb@ZIF-8 NP surface was saturated at 2 mg per mL PLL. Therefore, this concentration was selected for optimizing HSA deposition. Fig. 2a(ii) shows how, the addition of 1 mg per mL HSA, resulted in a ζ-potential decrease of only ~5 mV. Increasing the HSA concentration to 2 mg mL^{-1} further decreased the ζ-potential by an additional 13 mV. However, when the HSA concentration was increased to 3 mg mL^{-1}, while a further decrease in ζ-potential was observed, it also led to NP disassembly, as evidenced by images taken after two washes in HEPES buffer. Consequently, 2 mg per mL HSA was chosen as the optimal concentration for subsequent GA crosslinking optimization.

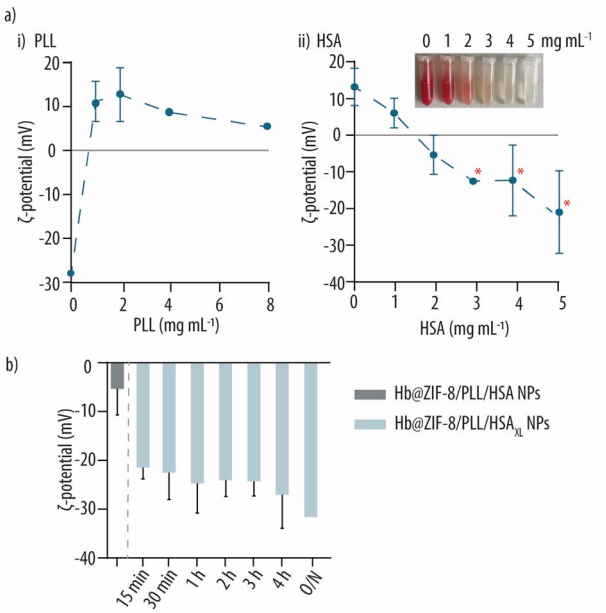

Fig. 2 (a) (i) Zeta (ζ)-potential measurements of Hb-loaded ZIF-8 NPs (Hb@ZIF-8 NPs) incubated with increasing concentrations of poly-L-lysine (PLL). (ii) ζ-potential measurements of PLL-coated Hb@ZIF-8 NPs incubated with increasing concentrations of human serum albumin (HSA), along with photographic images of the NP solutions at each HSA concentration after the final wash. The coating was conducted for 10 min in 10 mM HEPES buffer at pH 8.5. Data points marked with a red asterisk indicate HSA concentrations that resulted in NP disassembly. (b) ζ-potential measurements of PLL- and HSA-coated Hb@ZIF-8 NPs (*i.e.*, Hb@ZIF-8/PLL/HSA NPs) and after incubation with 1 mM glutaraldehyde (GA) in MQ for different time intervals. The crosslinked NPs are denoted as Hb@ZIF-8/PLL/HSA_{XL} NPs, where the subscript 'XL' indicates HSA crosslinking with GA after deposition, and O/N stands for overnight incubation.

Since, in these initial experiments the crosslinking step was conducted by incubating Hb@ZIF-8/PLL/HSA NPs with GA for 4 h, our next aim was to reduce the GA incubation time to accelerate NP preparation. Shortening the crosslinking duration is particularly beneficial for preserving Hb functionality, as GA can also react with Hb amine groups.[37] In fact, Prapan *et al.* reported that prolonged GA crosslinking in Hb submicron particles resulted in reduced oxyHb content, indicating compromised Hb functionality.[38] In agreement with Fig. 1b(i), incubation with GA led to the expected decrease in ζ-potential, consistent with GA reacting with amino groups to form imines *via* Schiff base formation (Fig. 2b). While slight variations in ζ-potential were observed across different incubation times, longer incubation generally resulted in lower ζ-potential values. However, these differences were negligible, as indicated by the overlapping error bars. Thus, the shortest incubation time of 15 min was selected as the optimal crosslinking duration, as it effectively stabilizes HSA while minimizing potential adverse effects on Hb functionality.

The addition of HSA to PLL-coated Hb@ZIF-8 NPs (Hb@ZIF-8/PLL NPs) resulted in significant Hb release, likely due to NP degradation caused by HSA competing with Zn^{2+} ions in the ZIF-8 core. HSA plays a crucial role in Zn^{2+} transport in the human body, which could explain the increased Hb release observed at higher HSA concentrations (Fig. 2a(ii)).[39] To mitigate NP degradation upon HSA addition, an additional GA crosslinking step prior to HSA deposition was considered. Since PLL also contains amine groups, its crosslinking with GA was expected to enhance NP structural integrity, making them more resistant to the degradation caused by HSA–Zn^{2+} competition. To this end, Hb@ZIF-8/PLL NPs crosslinking was conducted, and this time the Hb : GA molar ratio was evaluated (Fig. 3a). Although the NPs retained an overall positive charge, as expected, increasing GA concentrations resulted in a reduction in the overall ζ-potential of Hb@ZIF-8/PLL NPs due to the occupation of amine groups by GA (Fig. 3a(i)). Importantly, increasing the Hb : GA ratio significantly reduced Hb loss during the washing steps following HSA addition, as it is shown in Fig. 3a(ii) after the first centrifugation. Specifically, at a Hb : GA molar ratio of 1 : 5, the Hb loss was 3.1 ± 0.1 mg (for a total of around 8 mg), whereas at

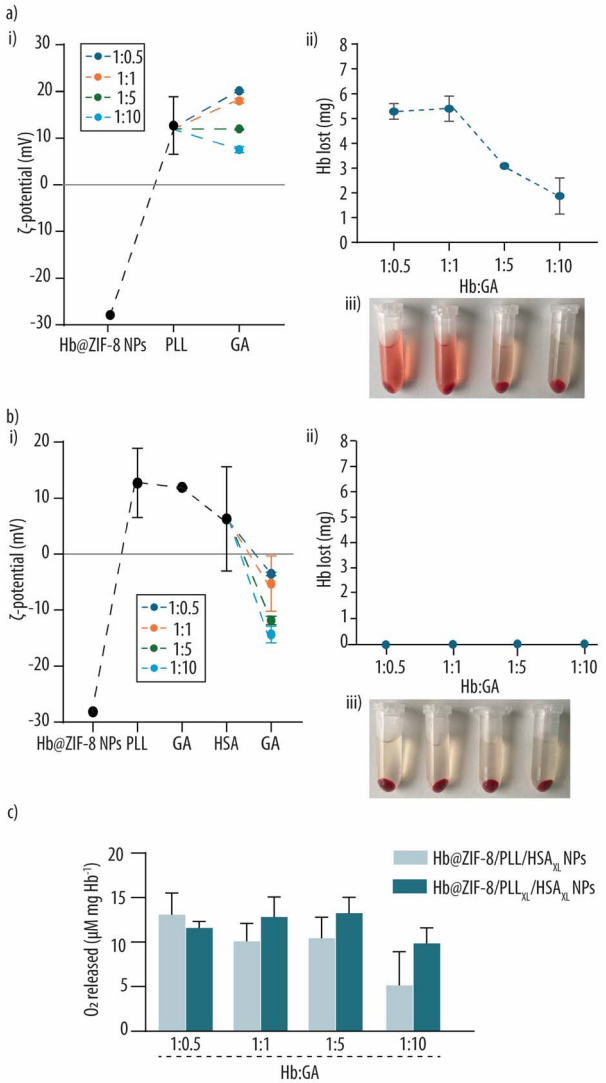

Fig. 3 (a) (i) Zeta (ζ)-potential measurements of Hb-loaded ZIF-8 NPs (Hb@ZIF-8 NPs) following deposition of poly-L-lysine (PLL) and crosslinking at various Hb : glutaraldehyde (GA) molar ratios (*i.e.*, Hb@ZIF-8/PLL_{XL} NPs), where the subscript 'XL' indicates PLL crosslinking with GA after deposition. (ii) Hb loss after the deposition of human serum albumin (HSA) onto Hb@ZIF-8/PLL_{XL} NPs. (iii) Photographic images taken after the first centrifugation step, showing HSA deposition onto Hb@ZIF-8/PLL_{XL} NPs crosslinked at different Hb : GA molar ratios. (b) (i) ζ-potential measurements of the stepwise assembly of HSA-coated Hb@ZIF-8/PLL_{XL} NPs (*i.e.*, Hb@ZIF-8/PLL_{XL}/HSA_{XL} NPs), where the subscript 'XL' indicates GA crosslinking after both PLL and HSA deposition. Several Hb : GA molar ratios were tested for HSA crosslinking. (ii) Hb loss after HSA crosslinking at different Hb : GA molar ratios and (iii) photographic images taken after the first centrifugation step, showing Hb@ZIF-8/PLL_{XL}/HSA_{XL} NPs crosslinked at different Hb : GA molar ratios. (c) Oxygen released per mg of Hb from Hb@ZIF-8/PLL/HSA_{XL} and Hb@ZIF-8/PLL_{XL}/HSA_{XL} NPs at different Hb : GA molar ratios.

1 : 10, this value decreased to 1.9 ± 0.7 mg. The reduced Hb losses at both 1 : 5 and 1 : 10 Hb : GA molar ratios were further supported by the very slightly red-colored supernatants of the Hb@ZIF-8/PLL_{XL}/HSA NPs after the first centrifugation step (Fig. 3a(iii)). Although the 1 : 10 Hb : GA molar ratio resulted in the lowest Hb loss, the 1 : 5 ratio was selected for further experiments, as it did not cause a significant decrease in ζ-potential, which could otherwise hinder the subsequent deposition of negatively charged HSA. Additionally, using a lower GA concentration is expected to better preserve Hb functionality by minimizing potential crosslinking interactions with Hb itself.

After identifying the optimal PLL crosslinking ratio, different Hb : GA molar ratios were also evaluated for the HSA coating step. As shown in Fig. 3b(i), Hb@ZIF-8/PLL_{XL}/HSA_{XL} NPs where the HSA had been crosslinked at Hb : GA molar ratios of 1 : 5 and 1 : 10 exhibited the lowest ζ-potentials, indicating higher HSA incorporation. Notably, no detectable Hb loss was observed for any of the tested Hb : GA molar ratios (Fig. 3b(ii)), consistent with photographic images of Hb@ZIF-8/PLL_{XL}/HSA_{XL} NPs taken after the first centrifugation step (Fig. 3b(iii)).

Despite being encapsulated within the NP core, Hb contains abundant amine groups and is expected to undergo partial crosslinking upon incubation with GA. Thus, we next assessed the potential impact of GA crosslinking on Hb functionality. Previous studies have reported that GA crosslinking can slightly reduce Hb's oxygen-binding capacity, while Wu *et al.* observed high levels of metHb formation during Hb polymerization with GA.[34,38] Therefore, we evaluated the oxygen release properties of Hb@ZIF-8/PLL/HSA_{XL} and Hb@ZIF-8/PLL_{XL}/HSA_{XL} NPs prepared with different Hb : GA ratios. To assess oxygen release and evaluate the effect of varying Hb : GA molar ratios, the NPs were incubated with $K_3[Fe(CN)_6]$, which converts Hb into metHb, thereby facilitating oxygen release. The amount of oxygen released was quantified using an oxygen electrode, and the results are shown in Fig. 3c, expressed as μM of oxygen released per mg of Hb. As observed, the oxygen released per mg of Hb ranges from 8–13 μM mg^{-1}. However, whether the NPs had been crosslinked once (for Hb@ZIF-8/PLL/HSA_{XL} NPs) or twice (Hb@ZIF-8/PLL_{XL}/HSA_{XL} NPs) did not have a marked effect on the amount of oxygen released. Likewise, increasing the Hb : GA ratio did not result in a marked decrease in oxygen release.

The oxygen release from the NPs normalized to that of an equivalent amount of free Hb is also presented (Fig. S2a, SI). However, direct comparison of oxygen release between Hb@ZIF-8/PLL/HSA_{XL} and Hb@ZIF-8/PLL_{XL}/HSA_{XL} NPs, free Hb, and Hb@ZIF-8 NPs may be misleading. Unlike free Hb and Hb@ZIF-8 NPs, which disassemble upon the addition of $K_3[Fe(CN)_6]$ and are instantly converted to metHb, the PLL and HSA-coated NPs remained intact, as shown in the photographic images after centrifugation (Fig. S2b, SI), suggesting that encapsulated Hb may not be fully converted to metHb. A more comprehensive assessment of Hb functionality, including oxygen-binding and release properties, is provided in Section 3.4.

Considering the ζ-potential values, Hb retention throughout the synthesis process, and oxygen release properties, we concluded that Hb@ZIF-8/PLL_{XL}/HSA_{XL} NPs crosslinked at a 1 : 5 Hb : GA molar ratio were optimal. Lower GA concentrations resulted in greater Hb loss and less negatively charged NPs, while higher Hb : GA ratios (*i.e.*, 1 : 10) did not provide any

additional improvements. Therefore, all subsequent experiments were conducted using the 1 : 5 Hb : GA molar ratio.

Upon determining the optimal Hb : GA molar ratio, the NPs were further characterized, with the results summarized in Fig. 4a. Both Hb@ZIF-8/PLL/HSA_{XL} NPs and Hb@ZIF-8/PLL_{XL}/HSA_{XL} NPs exhibit similarly negative surface charges (*i.e.* −25 mV). Notably, the Hb@ZIF-8/PLL_{XL}/HSA_{XL} NPs demonstrated a significantly higher EE of 54.2%, nearly double that of the Hb@ZIF-8/PLL/HSA_{XL} NPs (27.0%; $p < 0.05$). These results indicate that the additional crosslinking step following both PLL and HSA deposition stabilizes the NPs, thereby reducing Hb loss during fabrication. Cryo-SEM micrographs of Hb@ZIF-8/PLL_{XL}/HSA_{XL} NPs (Fig. 4b) show that the NPs display a well-defined spherical morphology, very similar to their uncoated counterparts (Fig. 1a), with an average diameter of ~316 nm, as indicated by the size histogram. This size is within the optimal range for HBOCs, which must remain in circulation for extended periods. To prevent extravasation through endothelial gaps into the underlying smooth muscle tissue—where they could bind and scavenge nitric oxide, leading to vasoconstriction—HBOCs should be larger than 100 nm.[35] However, carriers in the 2–3 μm range are susceptible to phagocytosis, and may obstruct microcirculation at higher concentrations.[40] Additionally, larger HBOCs have been linked to an increased risk of coagulopathy.[41] Thus, an optimal HBOC size range of 100–1000 nm ensures safe systemic delivery while minimizing adverse vascular effects.

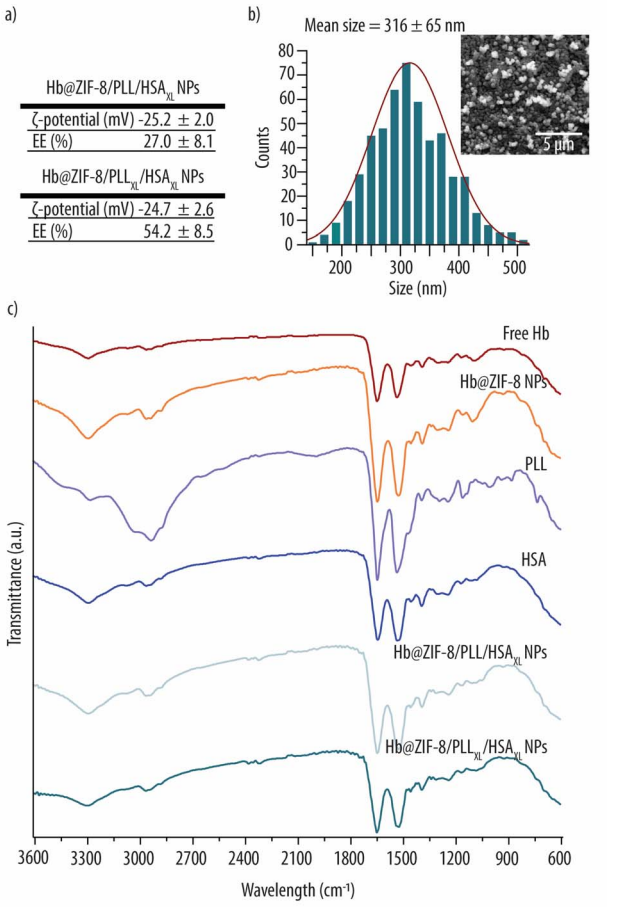

Fig. 4 (a) Table with zeta (ζ)-potential measurements and encapsulation efficiency (EE) of poly-L-lysine (PLL)- and human serum albumin (HSA)-coated Hb-loaded ZIF-8 NPs (*i.e.*, Hb@ZIF-8/PLL/HSA_{XL} and Hb@ZIF-8/PLL_{XL}/HSA_{XL} NPs). Data are presented as mean values. (b) Cryo-SEM micrograph and corresponding size distribution histogram of Hb@ZIF-8/PLL_{XL}/HSA_{XL} NPs. (c) FTIR spectra of free Hb, Hb-loaded ZIF-8 NPs (*i.e.*, Hb@ZIF-8 NPs), PLL, HSA, Hb@ZIF-8/PLL/HSA_{XL} and Hb@ZIF-8/PLL_{XL}/HSA_{XL} NPs. The subscript 'XL' indicates crosslinking with glutaraldehyde following PLL and/or HSA deposition.

To further verify the incorporation of PLL and HSA into Hb@ZIF-8/PLL/HSA_{XL} and Hb@ZIF-8/PLL_{XL}/HSA_{XL} NPs, FTIR analysis was performed (Fig. 4b). The FTIR spectrum of free Hb displays the two characteristic peaks of proteins at approximately 1647 and 1535 cm^{-1}, corresponding to the C=O stretching vibration of the amide I band and the N–H bending vibration of the amide II band, respectively. An additional peak at 3286 cm^{-1}, associated with N–H stretching vibrations of amide A, is present but with lower intensity. Hb@ZIF-8 NPs exhibit also prominent amide I and II peaks due to the presence of Hb, along with peaks originating from the HmIm ligand at approximately 2993 cm^{-1}, which are attributed to the stretching vibrations of aromatic C–H bonds in the imidazole ring. Being a polypeptide, the spectrum of PLL shows bands similar to those of Hb; a band at 2928 cm^{-1} corresponding to $-CH_2$ vibration absorption, along with peaks at 1643 and 1535 cm^{-1}. Specifically, the 1643 cm^{-1} peak corresponds to the C=O stretching vibration of the amide I band, while the 1535 cm^{-1} peak is attributed to the in-plane deformation of the N–H group in the amide II band. HSA, as expected, exhibits the characteristic spectral features of proteins, with characteristic amide I and II bands at approximately 1644 and 1530 cm^{-1}, respectively. Thus, the spectral overlap among the different components complicates direct confirmation of PLL and HSA incorporation into Hb@ZIF-8 NPs. Despite this, the observed changes in ζ-potential values provide strong evidence for the successful deposition of these components.

3.2. Assessment of NPs stability in different solvents and physiologically relevant media

A major challenge in the development of MOFs for biomedical applications is their susceptibility to degradation under physiologically relevant conditions. ZIF-8-based NPs are no exception—they are known to degrade in commonly used biological buffers such as PBS and in cell culture media.[42] To address this, we investigated whether coating Hb@ZIF-8 NPs with PLL and HSA could enhance their stability in various solvents, including biologically relevant solutions. To this end, Hb@ZIF-8/PLL/HSA_{XL} and Hb@ZIF-8/PLL_{XL}/HSA_{XL} NPs were incubated in a range of buffers and media, including MQ, 0.9% NaCl, 25 mM HEPES pH 7.4, 10 mM HEPES pH 8.5, 10 mM HEPES pH 7.4 with 150 mM NaCl, 10 mM TRIS pH 7.4 with 150 mM NaCl, PBS, and DMEM for up to 7 days. Hb release was quantified over time and compared to that of uncoated Hb@ZIF-8 NPs. All incubations were performed at 4 °C, except for DMEM, which was incubated at 37 °C to mimic *in vitro* conditions. As shown in

Fig. 5a(i), uncoated Hb@ZIF-8 NPs rapidly degraded in both PBS and DMEM, releasing ~80% of their Hb content within the first hour. No further increase in Hb release was observed with prolonged incubation. This rapid degradation was visually confirmed by the disappearance of the Hb@ZIF-8 NPs pellet and the appearance of a homogeneous red solution after 1 day of incubation in PBS or DMEM—characteristic of solubilized Hb (Fig. 5a(ii)). Interestingly, after 7 days in DMEM, a decrease in Hb release was observed for Hb@ZIF-8 NPs—an unexpected result, given that the assay measured cumulative release. We attribute this reduction to the oxidation of Hb to metHb, followed by potential dissociation into free heme and αβ-globin dimers, processes that are likely accelerated at 37 °C.[43] This hypothesis is supported by the brown coloration of the suspension after 7 days of incubation (Fig. S3, SI), consistent with metHb formation. For an accurate quantification of the Hb released in this case, a standard curve of metHb was prepared by measuring the Abs at 404 nm using the Nanodrop (Fig. S4, SI). Hb@ZIF-8/PLL/HSA_{XL} NPs showed only slightly improved stability in PBS and DMEM, releasing ~65% and 55% of their Hb content within 1 h, respectively (Fig. 5b(i)). As with Hb@ZIF-8 NPs, a decrease in measured Hb content was observed at later time points in DMEM, likely due to the same Hb oxidation/degradation mechanisms. Surprisingly, Hb@ZIF-8/PLL/HSA_{XL} NPs were less stable than their uncoated counterparts in other media, including 0.9% NaCl, 10 mM HEPES pH 7.4 with 150 mM NaCl, 10 mM TRIS pH 7.4 with 150 mM NaCl, where ~20% Hb release was detected after only 1 day. In contrast, Hb@ZIF-8/PLL_{XL}/HSA_{XL} NPs demonstrated markedly enhanced stability in all tested media, including PBS and DMEM (Fig. 5c(i)). After 1 day of incubation, only 20% and 22% of Hb was released in PBS and DMEM, respectively. For comparison, Hb release in DMEM was 71% for Hb@ZIF-8 NPs and 55% for Hb@ZIF-8/PLL/HSA_{XL} NPs. A similar trend to that observed for Hb@ZIF-8/PLL/HSA_{XL} NPs in NaCl-containing buffers was noted for Hb@ZIF-8/PLL_{XL}/HSA_{XL} NPs, however the extent of Hb release was significantly lower. These results confirm that crosslinking both the PLL and HSA layers with GA significantly improves NP structural integrity, enhancing their stability across physiologically relevant conditions and thereby increasing their potential for biological applications.

3.3. Evaluation of the stealth properties

The adsorption of serum proteins onto the surface of nanocarriers leads to the formation of a protein corona, which is rapidly recognized by the immune system. This recognition results in NPs clearance and, consequently, reduced circulation time.[44] In particular, opsonins such as IgG can bind to NP surfaces and promote phagocytosis through interactions with Fc receptors on immune cells. In contrast, other serum proteins like albumin may also adsorb onto NPs but do not elicit immune responses. These are referred to as dysopsonins.[45]

Until recently, PEG was widely regarded as the gold standard for NP coatings to reduce immunogenicity. However, an increasing number of studies have reported the presence of anti-PEG antibodies—immune components that specifically recognize and bind to PEG—thereby diminishing its protective efficacy.[46] As a result, alternative surface coatings have been investigated to prevent protein adsorption and immune recognition. Among them, serum albumins have emerged as promising candidates. For instance, Yu *et al.* demonstrated that BSA coatings on iron oxide NPs effectively prevented protein adsorption,[47] while Sato *et al.* showed that HSA-coated liposomes resisted phagocytosis compared to uncoated counterparts.[48]

In this study, we evaluated the efficacy of HSA coatings in preventing opsonin adsorption and promoting dysopsonin binding. To this end, Hb@ZIF-8/PLL/HSA_{XL} and Hb@ZIF-8/

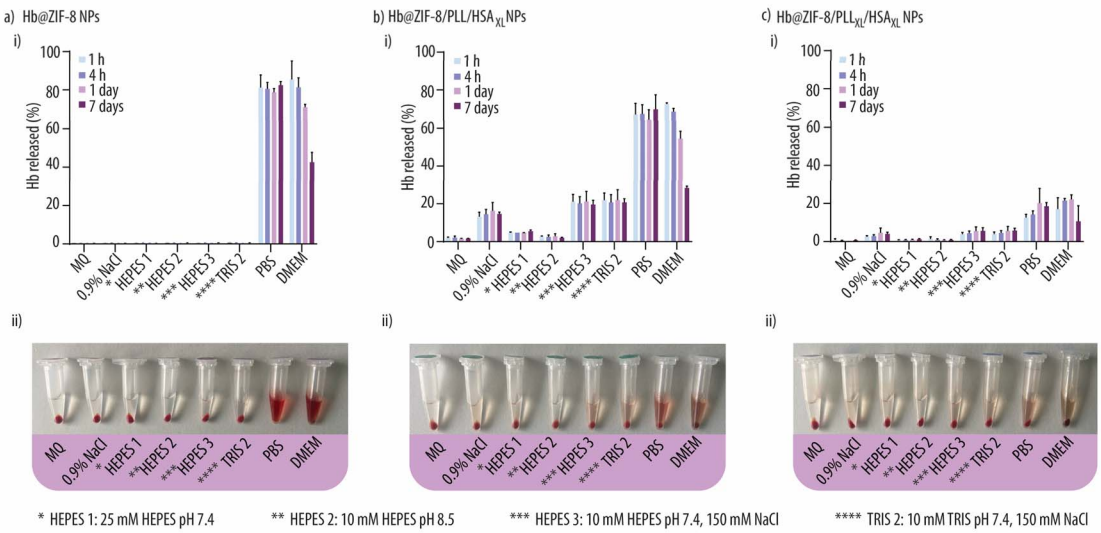

Fig. 5 Cumulative Hb release in various physiologically relevant media after incubation of: (a) bare Hb-loaded ZIF-8 NPs (Hb@ZIF-8 NPs) and poly-L-lysine (PLL)- and human serum albumin (HSA)-coated Hb@ZIF-8 NPs, denoted as (b) Hb@ZIF-8/PLL/HSA_{XL} and (c) Hb@ZIF-8/PLL_{XL}/HSA_{XL} NPs, where the subscript 'XL' indicates crosslinking with glutaraldehyde following PLL and/or HSA deposition.

PLL_{XL}/HSA_{XL} NPs were incubated with 0.5 mg mL^{-1} of either BSA-FITC or IgG-FITC in 10 mM HEPES buffer pH 7.4 containing 150 mM NaCl, to better mimic physiological ionic strength. Incubations were conducted for 4 h at 37 °C under continuous shaking. Hb@ZIF-8/PEG NPs were included as a positive control, based on our previous report demonstrating their antifouling properties.[17] Uncoated Hb@ZIF-8 NPs were excluded due to their decomposition under the conditions of the experimental setup. To quantify protein adsorption, standard curves of BSA-FITC and IgG-FITC were generated (Fig. S5a, SI). Fig. 6 summarizes the results of protein adsorption. Hb@ZIF-8/PEG NPs exhibited the lowest levels of BSA-FITC deposition, with approximately ~0.25 mg per mL BSA-FITC adsorbed from an initial concentration of 0.5 mg mL^{-1} (for 0.5 mg per mL Hb@ZIF-8/PEG NPs). Notably, increasing the NP concentration did not yield a proportional increase in BSA-FITC adsorption, suggesting that BSA-FITC was fully adsorbed even at the lowest NP concentration. To further probe differences among the NP formulations, higher concentrations of BSA-FITC (*i.e.*, 0.5, 2 and 5 mg mL^{-1}) were incubated with 2 mg per mL NPs under the same conditions. As shown in Fig. S5b, increasing the BSA-FITC concentration did not significantly enhance adsorption, and no notable differences were observed across NP types. These results suggest that both HSA and PEG coating have a similar effect on BSA-FITC adsorption.

In contrast, IgG-FITC adsorption displayed a concentration-dependent trend. Increasing the NP concentration led to higher IgG-FITC adsorption. Hb@ZIF-8/PEG NPs showed the highest IgG-FITC binding (~0.4 mg mL^{-1} at 2 mg per mL NP concentration). In comparison, IgG-FITC adsorption onto Hb@ZIF-8/PLL/HSA_{XL} and Hb@ZIF-8/PLL_{XL}/HSA_{XL} NPs was negligible at NP concentrations up to 1 mg mL^{-1}. At the highest tested NP concentration (2 mg mL^{-1}), IgG-FITC adsorption was only 0.07 and 0.02 mg mL^{-1} for Hb@ZIF-8/PLL/HSA_{XL} and Hb@ZIF-8/PLL_{XL}/HSA_{XL} NPs, respectively-more than five times lower than that of PEG-coated NPs. These findings underscore the superior antifouling performance of the HSA coating compared to our previously used PEG strategy.[17]

One possible explanation for this difference is the variation in coating density on the NP surface. Specifically, fewer PEG molecules may be incorporated into Hb@ZIF-8 NPs compared to HSA, reducing the overall effectiveness of PEG in providing stealth properties.

To further support the role of HSA coating in modulating protein adsorption, we measured the ζ-potential of the NPs in 10× diluted 10 mM HEPES pH 7.4 150 mM NaCl. As shown in Fig. S6 (SI), all NPs exhibited a slightly negative surface charge. This suggests that the differences in protein adsorption are not driven by electrostatic interactions with negatively charged proteins (IgG and BSA), but rather by the efficacy of HSA coating.

In summary, HSA coatings significantly improved the stealth properties of Hb@ZIF-8 NPs by markedly reducing IgG adsorption while maintaining BSA binding. These results indicate strong potential for prolonged circulation times and reduced immune clearance of HSA-coated NPs *in vivo*.

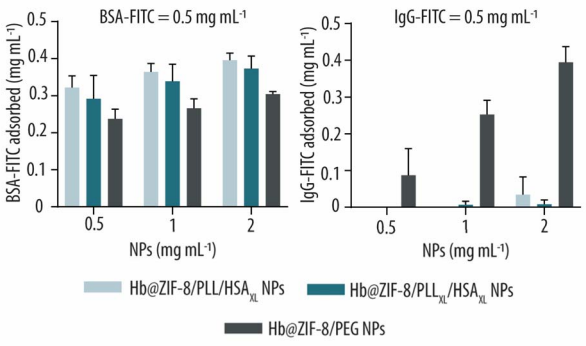

Fig. 6 Fluorescein 5(6) – Isothiocyanate (FITC)-labelled bovine serum albumin (BSA-FITC) and Immunoglobin G (IgG-FITC) adsorbed onto increasing concentrations of Hb-loaded ZIF-8 NPs (Hb@ZIF-8 NPs) coated with poly-L-lysine (PLL)- and human serum albumin (HSA), or polyethylene glycol (PEG)-coated Hb@ZIF-8 NPs (Hb@ZIF-8/PEG NPs). The PLL- and HSA-coated NPs are denoted as Hb@ZIF-8/PLL/HSA_{XL} and Hb@ZIF-8/PLL_{XL}/HSA_{XL} NPs, where the subscript 'XL' indicates glutaraldehyde crosslinking following PLL and/or HSA deposition.

3.4. Hb functionality assessment

Next, we assessed whether Hb retained its functional properties when encapsulated within the Hb@ZIF-8/PLL/HSA_{XL} and Hb@ZIF-8/PLL_{XL}/HSA_{XL} NPs. To do that, we analyzed its UV-Vis spectrum, which offers key insights into both the structural integrity and oxygenation state of Hb. Native Hb exhibits a characteristic absorption profile featuring a strong Soret peak around 415 nm corresponding to the heme group, along with two weaker Q-bands between 500–600 nm, related to the electronic transitions within the heme group. As shown in Fig. 7a, free oxyHb displays a prominent Soret peak at 414 nm, with two Q-bands at 541 and 576 nm. Upon deoxygenation, induced by the addition of SDT—an oxygen scavenger—, the Soret peak undergoes a red shift to 425 nm, while the two Q-bands merge into a single peak at 550 nm. This spectral shift confirms the successful deoxygenation of Hb and takes place for an additional cycle of oxygenation and deoxygenation.

In the case of both Hb@ZIF-8/PLL/HSA_{XL} and Hb@ZIF-8/PLL_{XL}/HSA_{XL} NPs, the oxygenation–deoxygenation spectral response of encapsulated Hb closely mirrors that of free Hb. This indicates that Hb retains its functionality throughout the fabrication process. Specifically, for Hb@ZIF-8/PLL/HSA_{XL} NPs, the Soret peak shifted from 413 to 416 nm during deoxygenation, while for Hb@ZIF-8/PLL_{XL}/HSA_{XL} NPs, it shifted from 416 to 423 nm. However, a sloping baseline was observed at lower wavelengths in the spectra of both coated NPs, likely due to light scattering effects associated with the presence of intact NPs.[49] This scattering reduced the resolution of the Q-bands during the deoxygenation cycle, making them more difficult to distinguish. Notably, the spectra of uncoated Hb@ZIF-8 NPs could not be obtained due to their instability in the presence of SDT. Despite this, the observed red and blue shifts of Soret peak during both oxygenation and deoxygenation cycles confirm that

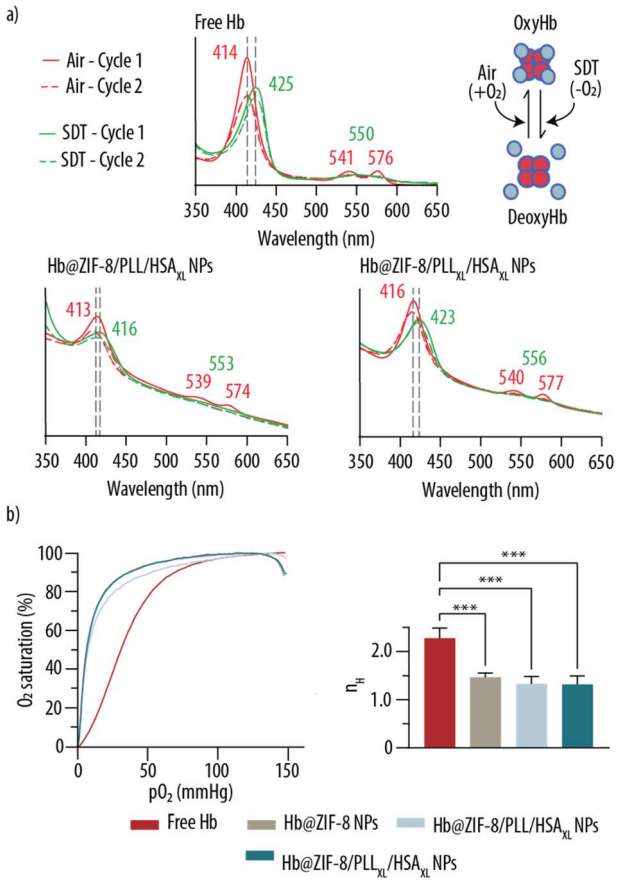

	p50 (mmHg)	n_H
Free Hb	30.7±0.3	2.3±0.2
Hb@ZIF-8 NPs	4.9±0.4	1.5±0.0
Hb@ZIF-8/PLL/HSA_{XL} NPs	6.4±0.6	1.4±0.2
Hb@ZIF-8/PLL_{XL}/HSA_{XL} NPs	5.4±0.0	1.4±0.2

Fig. 7 (a) UV-vis spectra of free Hb, Hb-loaded ZIF-8 NPs (Hb@ZIF-8 NPs) coated with poly-L-lysine (PLL)- and human serum albumin (HSA) after treatment with compressed air or sodium dithionite (SDT) to generate oxygenated (oxyHb) and deoxygenated (deoxyHb) forms, respectively. (b) Oxygen dissociation curve showing the oxygen saturation as a function of the partial oxygen pressure (pO_2) along with the $p50$ (pO_2 at which Hb is 50% saturated with oxygen) and Hill coefficient (n_H) values of free Hb and the different NPs, with statistical significance indicated (***$p < 0.001$). The NPs are denoted as Hb@ZIF-8/PLL/HSA_{XL} and Hb@ZIF-8/PLL_{XL}/HSA_{XL} NPs, where the subscript 'XL' indicates glutaraldehyde crosslinking following PLL and/or HSA deposition.

the oxygen-binding and -releasing capabilities were preserved within all coated NPs.

To further evaluate Hb functionality, we determined the ODCs of the Hb@ZIF-8/PLL/HSA_{XL} and Hb@ZIF-8/PLL_{XL}/HSA_{XL} NPs. As shown in Fig. 7b, free Hb displayed a $p50$ value of 30.7 mmHg, slightly higher than the commonly reported value for bovine Hb (26.3 mmHg) and native human Hb within RBCs (25.6 mmHg).[50] In contrast, markedly lower $p50$ values were observed for Hb@ZIF-8 (4.9 mmHg), Hb@ZIF-8/PLL/HSA_{XL} (6.4 mmHg) and Hb@ZIF-8/PLL_{XL}/HSA_{XL} NPs (5.4 mmHg), indicating enhanced oxygen affinity. This phenomenon has been previously attributed to the presence of the imidazole-containing HmIm linker in ZIF-8, which may mimic histidine residues and stabilize the oxygen bound to the heme group through coordination interactions.[15,16] Additionally, n_H values for all NPs were statistically significantly lower than that of free Hb (2.3), with values close to 1.5 ($p < 0.001$). This reduction can be attributed to Hb encapsulation, as unmodified and modified NPs display very similar n_H values with no statistical differences (Fig. S7, SI). Although reduced, these n_H values still suggest the presence of positive cooperativity in oxygen binding. Taken together, these results suggest that Hb@ZIF-8/PLL/HSA_{XL} and Hb@ZIF-8/PLL_{XL}/HSA_{XL} NPs maintain key aspects of Hb functionality and are promising candidates for use as artificial oxygen carriers.

3.5. Biocompatibility assessment

The last objective of this study was to evaluate the biocompatibility of Hb@ZIF-8/PLL_{XL}/HSA_{XL} NPs to determine their suitability for biological applications. This assessment was conducted using an *in vitro* model based on the RAW 264.7 murine macrophage cell line. This cell line was chosen due to macrophages' critical role in immune responses through its involvement in phagocytosis and pathogen clearance.[51]

The biocompatibility study focused exclusively on Hb@ZIF-8/PLL_{XL}/HSA_{XL} NPs, as they demonstrated superior stability in both PBS and DMEM (see Fig. 5), with significantly reduced Hb release compared to Hb@ZIF-8 and Hb@ZIF-8/PLL/HSA_{XL} NPs. RAW 264.7 cells were incubated with varying concentrations of Hb@ZIF-8/PLL_{XL}/HSA_{XL} NPs (100 μL, 0–5 mg mL^{-1}) at 37 °C in a humidified incubator with 5% CO_2 for 24 h, as indicated by the ISO 10993-5 guidelines.[52] As shown in Fig. 8, most concentrations resulted in nCV above 70%, indicated by the light pink dashed line representing the minimum acceptable threshold

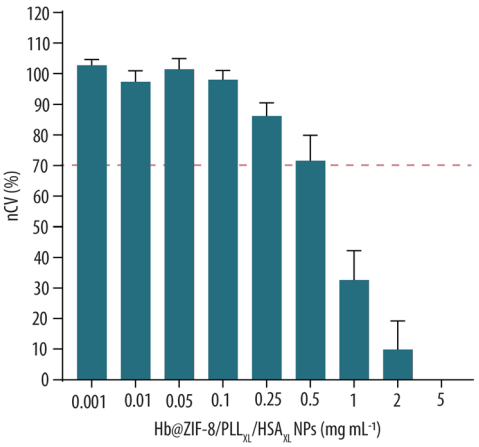

Fig. 8 Normalized cell viability (nCV) of RAW 264.7 cells following incubation for 24 h with increasing concentrations of poly-L-lysine (PLL)- and human serum albumin (HSA)-coated Hb-loaded ZIF-8 NPs. The dashed line indicates the 70% viability threshold defined by ISO 10993-5 for classifying materials as non-cytotoxic. The NPs are denoted as Hb@ZIF-8/PLL_{XL}/HSA_{XL} NPs where the subscript 'XL' indicates glutaraldehyde crosslinking following PLL and HSA deposition.

for materials with a biological application, as defined by the ISO 10993-5 guidelines.[52] Hb@ZIF-8/PLL_{XL}/HSA_{XL} NPs were shown to be cytotoxic at concentrations exceeding 0.5 mg mL^{-1}. At exactly 0.5 mg mL^{-1}, the nCV was 71.6 ± 8.3%, placing it just at the ISO threshold. This suggests that a lower concentration, such as 0.25 mg mL^{-1}, would offer a safer biocompatibility profile. As NPs concentration increased, nCV progressively decreased. This decline may be attributed to a potential release of Zn^{2+} from the ZIF-8 core. Elevated intracellular Zn^{2+} levels are known to induce cytotoxic effects. For instance, Chen *et al.* reported that the majority of ZIF-8 NP-induced cytotoxicity in human cell lines stemmed from Zn^{2+} accumulation.[53] Notably, when comparing our results to those reported in the literature for similar systems based on ZIF-8 NPs, Hb@ZIF-8/PLL_{XL}/HSA_{XL} NPs exhibited superior biocompatibility. For example, Gu *et al.* studied uncoated ZIF-8 NPs loaded with bovine Hb and observed a nCV of approximately 40% after 24 h incubation, at a NP concentration of just 0.2 mg mL^{-1}. Similarly, Johari *et al.* assessed the cytotoxicity of ZIF-8 NPs to eukaryotic cell lines after 24 h incubation and found that exposure to 0.25 mg per mL ZIF-8 NPs led to a CV lower than 20%.[50,54] In contrast, our Hb@ZIF-8/PLL_{XL}/HSA_{XL} NPs maintained more than 70% CV at concentrations twice as high, highlighting the significant improvement in safety. Hb@ZIF-8/PEG NPs, previously reported by our group, were an exception, demonstrating a CV of approximately 95% at a 2 mg per mL NP concentration. However, this study was conducted under a shorter incubation period of only 4 h, making it difficult to directly compare to the current study.

These findings underscore the benefit of HSA coating in enhancing Hb@ZIF-8 NPs stability and biocompatibility.

4. Conclusions

In this study, we developed and optimized HSA-coated Hb@ZIF-8 NPs (Hb@ZIF-8/PLL_{XL}/HSA_{XL} NPs) with enhanced structural stability, stealth properties, and preserved oxygen-carrying functionality. By employing a systematic approach that included PLL bridging, HSA surface functionalization and GA crosslinking, we addressed several of the physicochemical limitations observed in earlier HBOC formulations.

Compared to PEGylated counterparts, our HSA-coated Hb@ZIF-8 NPs demonstrated improved colloidal stability in physiologically relevant media, reduced opsonin (*i.e.*, IgG) adsorption, and high retention of dysopsonin (*i.e.*, BSA) binding, suggesting improved immune evasion potential. Importantly, oxygen-binding and -release behavior remained comparable to that of free Hb, with ODCs confirming preserved cooperativity albeit with increased oxygen affinity—an expected effect of the ZIF-8 environment. Notably, this relatively low $p50$ values observed may be advantageous in contexts such as ischemia or stroke, where high-affinity carriers can preserve O_2 during circulation and preferentially unload it in severely hypoxic tissues.

Preliminary cytotoxicity assays in macrophage cultures further indicated a favorable biocompatibility profile of Hb@ZIF-8/PLL_{XL}/HSA_{XL} NPs compared to previously reported ZIF-8-based HBOCs.

While these findings highlight the promise of Hb@ZIF-8/PLL_{XL}/HSA_{XL} NPs as a next-generation HBOC platform, we recognize that our conclusions are confined to *in vitro* physicochemical and functional assessments. Comprehensive *in vitro* and *in vivo* studies—including evaluations of cellular uptake, intracellular processing, clearance pathways, biodistribution, pharmacokinetics, and therapeutic efficacy—will be essential to fully establish the biological fate and safety profile of this formulation.

Taken together, this work provides an encouraging foundation for future investigations aimed at advancing safer, more effective, and longer-circulating artificial oxygen carriers for transfusion medicine and hypoxia-related therapies.

Author contributions

The manuscript was written through contributions of all authors. All authors have given approval to the final version of the manuscript.

Conflicts of interest

There are no conflicts to declare.

Data availability

Additional data sets used and/or analyzed during the current study are available from the corresponding author upon reasonable request.

All data generated or analyzed during this study are included in this published article and its supplementary information (SI). Supplementary information is available. See DOI: **https://doi.org/10.1039/d5na00677e**.

Acknowledgements

This research was funded by the European Research Council under the European Union's Horizon 2020 Research and Innovation Program (Grant No. 101002060). During the preparation of this work the authors used Chat GPT in order to improve the readability of the manuscript. After using this tool/service, the authors reviewed and edited the content as needed and take full responsibility for the content of the publication.

References

1 C. Coll-Satue, S. Bishnoi, J. Chen and L. Hosta-Rigau, Stepping Stones to the Future of Haemoglobin-Based Blood Products: Clinical, Preclinical and Innovative Examples, *Biomater. Sci.*, 2021, **9**(4), 1135–1152, DOI: **10.1039/d0bm01767a**.

2 A. Sen Gupta, Hemoglobin-Based Oxygen Carriers: Current State-of-the-Art and Novel Molecules, *Shock*, 2019, **52**(1S), 70–83, DOI: **10.1097/shk.0000000000001009**.

3 M. M. T. Jansman and L. Hosta-Rigau, Recent and Prominent Examples of Nano- and Microarchitectures as Hemoglobin-Based Oxygen Carriers, *Adv. Colloid Interface Sci.*, 2018, **260**, 65–84, DOI: **10.1016/j.cis.2018.08.006**.

4 J. Chen, X. Liu, M. M. T. Jansman, P. W. Thulstrup and L. Hosta-Rigau, Metal-Phenolic Networks as Broad-Spectrum Antioxidant Coatings for Hemoglobin Nanoparticles Working as Oxygen Carriers, *Chem. Mater.*, 2022, **34**(20), 9200–9211, DOI: **10.1021/acs.chemmater.2c02190**.

5 T. M. S. Chang, Blood Substitutes Based on Nanobiotechnology, *Trends Biotechnol.*, 2006, **24**(8), 372–377, DOI: **10.1016/j.tibtech.2006.06.005**.

6 X. Liu, M. M. T. Jansman, P. W. Thulstrup, A. C. Mendes, I. S. Chronakis and L. Hosta-Rigau, Low-Fouling Electrosprayed Hemoglobin Nanoparticles with Antioxidant Protection as Promising Oxygen Carriers, *Macromol. Biosci.*, 2020, **20**(2), 1900293, DOI: **10.1002/mabi.201900293**.

7 X. Liu, M. M. T. Jansman, W. Li, P. Kempen, P. W. Thulstrup and L. Hosta-Rigau, Metal-Organic Framework-Based Oxygen Carriers with Antioxidant Protection as a Result of a Polydopamine Coating, *Biomater. Sci.*, 2021, **9**(21), 7257–7274, DOI: **10.1039/d1bm01005k**.

8 H. Liu, C. Yan, K. Yan, W. Zhu, Y. Shen, B. Yang, C. Chen and H. Zhu, Study of the Effects of Polymerized Porcine Hemoglobin (PPolyHb) in an Acute Anemia Rat Model, *Artif. Cells, Nanomed., Biotechnol.*, 2017, **45**(4), 694–700, DOI: **10.1080/21691401.2016.1228665**.

9 T. J. Styslinger, N. Zhang, V. S. Bhatt, N. Pettit, A. F. Palmer and P. G. Wang, Site-Selective Glycosylation of Hemoglobin with Variable Molecular Weight Oligosaccharides: Potential Alternative to PEGylation, *J. Am. Chem. Soc.*, 2012, **134**(17), 7507–7515, DOI: **10.1021/ja300893t**.

10 H. Azuma, T. Amano, N. Kamiyama, N. Takehara, M. Jingu, H. Takagi, O. Sugita, N. Kobayashi, T. Kure, T. Shimizu, T. Ishida, M. Matsumoto and H. Sakai, First-in-Human Phase 1 Trial of Hemoglobin Vesicles as Artificial Red Blood Cells Developed for Use as a Transfusion Alternative, *Blood Adv.*, 2022, **6**(21), 5711–5715, DOI: **10.1182/bloodadvances.2022007977**.

11 D. A. Belcher, C. T. Cuddington, E. L. Martindale, I. S. Pires and A. F. Palmer, Controlled Polymerization and Ultrafiltration Increase the Consistency of Polymerized Hemoglobin for Use as an Oxygen Carrier, *Bioconjug. Chem.*, 2020, **31**(3), 605–621, DOI: **10.1021/acs.bioconjchem.9b00766**.

12 K. D. Vandegriff, M. A. Young, P. E. Keipert and R. M. Winslow, The Safety Profile of Hemospan ® : A New Oxygen Therapeutic Designed Using Maleimide Poly(Ethylene) Glycol Conjugation to Human Hemoglobin, *Transfus. Altern. Transfus. Med.*, 2007, **9**(4), 213–225, DOI: **10.1111/j.1778-428x.2007.00083.x**.

13 S. Rameez and A. F. Palmer, Simple Method for Preparing Poly(Ethylene Glycol)-Surface-Conjugated Liposome-Encapsulated Hemoglobins: Physicochemical Properties, Long-Term Storage Stability, and Their Reactions with O2, CO, and NO, *Langmuir*, 2011, **27**(14), 8829–8840, DOI: **10.1021/la201246m**.

14 X. Gu and A. F. Palmer, ZIF-8 Metal-Organic Framework Nanoparticles Loaded with Hemoglobin as a Potential Red Blood Cell Substitute, *ACS Appl. Nano Mater.*, 2022, **5**(4), 5670–5679, DOI: **10.1021/acsanm.2c00608**.

15 D. Douka, W. Jin, C. Cantallops-Iglesias, A. Dieste-Izquierdo, P. W. Thulstrup and L. Hosta-Rigau, Optimization and Investigation of Hemoglobin-Loaded ZIF-90 Metal–Organic Framework Nanoparticles as Artificial Oxygen Carriers, *Part. Part. Syst. Charact.*, 2024, **42**(3), 2400189, DOI: **10.1002/ppsc.202400189**.

16 C. Coll-Satue, M. Rubio-Huertas, A. Ducrot, E. Norkute, X. Liu, F. M. Ebrahim, B. Smit, P. W. Thulstrup and L. Hosta-Rigau, A Novel PEG-Mediated Approach to Entrap Hemoglobin (Hb) within ZIF-8 Nanoparticles: Balancing Crystalline Structure, Hb Content and Functionality, *Biomater. Adv.*, 2024, **163**, 213953, DOI: **10.1016/j.bioadv.2024.213953**.

17 C. Coll-Satue, E. Cabrera-San Millan, M. M. T. Jansman, L. Arnholdt and L. Hosta-Rigau, Hemoglobin-Loaded ZIF-8 Nanoparticles Equipped with PEGylated Metal-Phenolic Network Coatings: An Oxygen Carrier with Antioxidant and Stealth Properties, *J. Mater. Chem. B*, 2025, **13**, 3374–3389, DOI: **10.1039/d4tb01771d**.

18 G. Bor, W. Jin, D. Douka, N. J. Borthwick, X. Liu, M. M. T. Jansman and L. Hosta-Rigau, In Vitro and in Vivo Investigations of Hemoglobin-Loaded PEGylated ZIF-8 Nanoparticles as Oxygen Carriers for Emergency Transfusion, *Biomater. Adv.*, 2025, **168**, 214118, DOI: **10.1016/j.bioadv.2024.214118**.

19 X. Liu, M. M. T. Jansman and L. Hosta-Rigau, Haemoglobin-Loaded Metal Organic Framework-Based Nanoparticles Camouflaged with a Red Blood Cell Membrane as Potential Oxygen Delivery Systems, *Biomater. Sci.*, 2020, **8**(21), 5859–5873, DOI: **10.1039/d0bm01118e**.

20 M. M. T. Jansman, C. Coll-Satue, X. Liu, P. J. Kempen, T. L. Andresen, P. W. Thulstrup and L. Hosta-Rigau, Hemoglobin-Based Oxygen Carriers Camouflaged with Membranes Extracted from Red Blood Cells: Optimization and Assessment of Functionality, *Biomater. Adv.*, 2022, **134**, 112691, DOI: **10.1016/j.msec.2022.11269**.

21 R. Wang, Z. Zhang, B. Liu, J. Xue, F. Liu, T. Tang, W. Liu, F. Feng and W. Qu, Strategies for the Design of Nanoparticles: Starting with Long-Circulating Nanoparticles, from Lab to Clinic, *Biomater. Sci.*, 2021, **9**(10), 3621–3637, DOI: **10.1039/d0bm02221g**.

22 S. Bozzer, M. C. Grimaldi, L. De Maso, M. Manfredi, G. Toffoli, M. Dal Bo, D. Sblattero and P. Macor, Stealth-Engineered Albumin-Coated Nanoparticles for Targeted Therapy: Effective Drug Delivery and Tumor Suppression in Xenograft-Zebrafish Model, *Int. J. Nanomed.*, 2024, **19**, 13267, DOI: **10.2147/ijn.s476241**.

23 J. Fu, E. Wu, G. Li, B. Wang and C. Zhan, Anti-PEG Antibodies: Current Situation and Countermeasures, *Nano Today*, 2024, **55**, 102163, DOI: **10.1016/j.nantod.2024.102163**.

24 X. Tao, Q. Zhang, K. Ling, Y. Chen, W. Yang, F. Gao and G. Shi, Effect of Pullulan Nanoparticle Surface Charges on HSA Complexation and Drug Release Behavior of HSA-Bound Nanoparticles, *PLoS One*, 2012, **7**(11), e49304, DOI: 10.1371/journal.pone.0049304.

25 H. Hyun, J. Park, K. Willis, J. E. Park, L. T. Lyle, W. Lee and Y. Yeo, Surface Modification of Polymer Nanoparticles with Native Albumin for Enhancing Drug Delivery to Solid Tumors, *Biomaterials*, 2018, **180**, 206–224, DOI: 10.1016/j.biomaterials.2018.07.024.

26 C. T. Privalle, C. J. Stacey and T. L. Talarico, Methods for the Synthesis of a Modified Hemoglobin Solution, *U.S. Pat.*, US6747132B2, 2004.

27 C. Coll-Satue, M. M. T. Jansman and L. Hosta-Rigau, Comparative Evaluation of UV-Vis Spectroscopy-Based Approaches for Hemoglobin Quantification: Method Selection and Practical Insights, *Biomolecules*, 2024, **14**(9), 1046, DOI: 10.3390/biom14091046.

28 M. Nadimifar, W. Jin, C. Coll-Satue, G. Bor, P. J. Kempen, A. A. Moosavi-Movahedi and L. Hosta-Rigau, Synthesis of Bioactive Hemoglobin-Based Oxygen Carrier Nanoparticles via Metal-Phenolic Complexation, *Biomater. Adv.*, 2024, **156**, 213698, DOI: 10.1016/j.bioadv.2023.213698.

29 M. M. T. Jansman, X. Liu, P. Kempen, G. Clergeaud, T. L. Andresen, P. W. Thulstrup and L. Hosta-Rigau, Hemoglobin-Based Oxygen Carriers Incorporating Nanozymes for the Depletion of Reactive Oxygen Species, *ACS Appl. Mater. Interfaces*, 2020, **12**(45), 50275–50286, DOI: 10.1021/acsami.0c14822.

30 Y. Komarova and A. B. Malik, Regulation of Endothelial Permeability via Paracellular and Transcellular Transport Pathways, *Annu. Rev. Physiol.*, 2010, **72**(1), 463–493, DOI: 10.1146/annurev-physiol-021909-135833.

31 Q. Peng, S. Zhang, Q. Yang, T. Zhang, X. Q. Wei, L. Jiang, C. L. Zhang, Q. M. Chen, Z. R. Zhang and Y. F. Lin, Preformed Albumin Corona, a Protective Coating for Nanoparticles Based Drug Delivery System, *Biomaterials*, 2013, **34**(33), 8521–8530, DOI: 10.1016/j.biomaterials.2013.07.102.

32 P. Batys, M. Morga, P. Bonarek and M. Sammalkorpi, PH-Induced Changes in Polypeptide Conformation: Force-Field Comparison with Experimental Validation, *J. Phys. Chem. B*, 2020, **124**(14), 2961–2972, DOI: 10.1021/acs.jpcb.0c01475.

33 M. Zheng, M. Pan, W. Zhang, H. Lin, S. Wu, C. Lu, S. Tang, D. Liu and J. Cai, Poly(α-L-Lysine)-Based Nanomaterials for Versatile Biomedical Applications: Current Advances and Perspectives, *Bioact. Mater.*, 2021, **6**(7), 1878–1909, DOI: 10.1016/j.bioactmat.2020.12.001.

34 M. Wu, K. Feng, Q. Li, H. Ma, H. Zhu, Y. Xie, G. Yan, C. Chen and K. Yan, Glutaraldehyde-Polymerized Hemoglobin and Tempol (PolyHb-Tempol) Has Superoxide Dismutase Activity That Can Attenuate Oxidative Stress on Endothelial Cells Induced by Superoxide Anion, *Artif. Cells, Nanomed., Biotechnol.*, 2018, **46**(1), 47–55, DOI: 10.1080/21691401.2017.1328685.

35 Y. Xiong, Z. Z. Liu, R. Georgieva, K. Smuda, A. Steffen, M. Sendeski, A. Voigt, A. Patzak and H. Bäumler, Nonvasoconstrictive Hemoglobin Particles as Oxygen Carriers, *ACS Nano*, 2013, **7**(9), 7454–7461, DOI: 10.1021/nn402073n.

36 A. D. Russell, Glutaraldehyde: Current Status and Uses, *Infect. Control Hosp. Epidemiol.*, 1994, **15**(11), 724–733, DOI: 10.1086/646845.

37 H. W. Sung, Y. Chang, C. T. Chiu, C. N. Chen and H. C. Liang, Crosslinking Characteristics and Mechanical Properties of a Bovine Pericardium Fixed with a Naturally Occurring Crosslinking Agent, *J. Biomed. Mater. Res.*, 1999, **47**(2), 116–126, DOI: 10.1002/(sici)1097-4636(199911)47:2<116::aid-jbm2>3.0.co;2-j.

38 A. Prapan, N. Suwannasom, C. Kloypan, S. Chaiwaree, A. Steffen, Y. Xiong, I. Kao, A. Prub, R. Georgieva and H. Bäumler, Surface Modification of Hemoglobin-Based Oxygen Carriers Reduces Recognition by Haptoglobin, Immunoglobulin, and Hemoglobin Antibodies, *Coatings*, 2019, **9**(7), 454, DOI: 10.3390/coatings9070454.

39 S. Al-Harthi, K. Chandra and Ł. Jaremko, Lipoic Acid Restores Binding of Zinc Ions to Human Serum Albumin, *Front. Chem.*, 2022, **10**, 942585, DOI: 10.3389/fchem.2022.942585.

40 J. A. Champion, A. Walker and S. Mitragotri, Role of Particle Size in Phagocytosis of Polymeric Microspheres, *Pharm. Res.*, 2008, **25**(8), 1815–1821, DOI: 10.1007/s11095-008-9562-y.

41 K. Roghani, R. Holtby and J. Jahr, Effects of Hemoglobin-Based Oxygen Carriers on Blood Coagulation, *J. Funct. Biomater.*, 2014, **5**(4), 288–295, DOI: 10.3390/jfb5040288.

42 M. D. J. Velásquez-Hernández, R. Ricco, F. Carraro, F. T. Limpoco, M. Linares-Moreau, E. Leitner, H. Wiltsche, J. Rattenberger, H. Schröttner, P. Frühwirt, E. M. Stadler, G. Gescheidt, H. Amenitsch, C. J. Doonan and P. Falcaro, Degradation of ZIF-8 in Phosphate Buffered Saline Media, *CrystEngComm*, 2019, **21**(31), 4538–4544, DOI: 10.1039/c9ce00757a.

43 J. M. Rifkind, J. G. Mohanty and E. Nagababu, The Pathophysiology of Extracellular Hemoglobin Associated with Enhanced Oxidative Reactions, *Front. Physiol.*, 2015, **5**, 500, DOI: 10.3389/fphys.2014.00500.

44 S. Schöttler, G. Becker, S. Winzen, T. Steinbach, K. Mohr, K. Landfester, V. Mailänder and F. R. Wurm, Protein Adsorption Is Required for Stealth Effect of Poly(Ethylene Glycol)- and Poly(Phosphoester)-Coated Nanocarriers, *Nat. Nanotechnol.*, 2016, **11**(4), 372–377, DOI: 10.1038/nnano.2015.330.

45 E. Papini, R. Tavano and F. Mancin, Opsonins and Dysopsonins of Nanoparticles: Facts, Concepts, and Methodological Guidelines, *Front. Immunol.*, 2020, **11**, 567365, DOI: 10.3389/fimmu.2020.567365.

46 P. Zhang, F. Sun, S. Liu and S. Jiang, Anti-PEG Antibodies in the Clinic: Current Issues and beyond PEGylation, *J. Contr. Release*, 2016, **244**, 184–193, DOI: 10.1016/j.jconrel.2016.06.040.

47 S. Yu, A. Perálvarez-Marín, C. Minelli, J. Faraudo, A. Roig and A. Laromaine, Albumin-Coated SPIONs: An Experimental

and Theoretical Evaluation of Protein Conformation, Binding Affinity and Competition with Serum Proteins, *Nanoscale*, 2016, **8**(30), 14393–14405, DOI: **10.1039/c6nr01732k**.

48 H. Sato, E. Nakhaei, T. Kawano, M. Murata, A. Kishimura, T. Mori and Y. Katayama, Ligand-Mediated Coating of Liposomes with Human Serum Albumin, *Langmuir*, 2018, **34**(6), 2324–2331, DOI: **10.1021/acs.langmuir.7b04024**.

49 J. Chen, M. M. T. Jansman, X. Liu and L. Hosta-Rigau, Synthesis of Nanoparticles Fully Made of Hemoglobin with Antioxidant Properties: A Step toward the Creation of Successful Oxygen Carriers, *Langmuir*, 2021, **37**(39), 11561–11572, DOI: **10.1021/acs.langmuir.1c01855**.

50 X. Gu, M. Allyn, K. Swindle-Reilly and A. F. Palmer, ZIF-8 Metal Organic Framework Nanoparticle Loaded with Tense Quaternary State Polymerized Bovine Hemoglobin: Potential Red Blood Cell Substitute with Antioxidant Properties, *Nanoscale*, 2023, **15**(19), 832–8844, DOI: **10.1039/d2nr06812e**.

51 B. Taciak, M. Białasek, A. Braniewska, Z. Sas, P. Sawicka, Ł. Kiraga, T. Rygiel and M. Król, Evaluation of Phenotypic and Functional Stability of RAW 264.7 Cell Line through Serial Passages, *PLoS One*, 2018, **13**(6), e0198943, DOI: **10.1371/journal.pone.0198943**.

52 International Organization for Standardization, *Biological Evaluation of Medical Devices – Tests for in Vitro Cytotoxicity*, ISO 10993-5:2009, 2009.

53 P. Chen, M. He, B. Chen and B. Hu, Size- and Dose-Dependent Cytotoxicity of ZIF-8 Based on Single Cell Analysis, *Ecotoxicol. Environ. Saf.*, 2020, **205**, 111110, DOI: **10.1016/j.ecoenv.2020.111110**.

54 S. A. Johari, M. Sarkheil and S. Veisi, Cytotoxicity, Oxidative Stress, and Apoptosis in Human Embryonic Kidney (HEK293) and Colon Cancer (SW480) Cell Lines Exposed to Nanoscale Zeolitic Imidazolate Framework 8 (ZIF-8), *Environ. Sci. Pollut. Res.*, 2021, **28**(40), 56772–56781, DOI: **10.1007/s11356-021-14636-5**.